UCLA
UCLA Previously Published Works

Title

Hypothalamic oestrogen receptor alpha establishes a sexually dimorphic regulatory node of energy expenditure

Permalink

https://escholarship.org/uc/item/3v043804

Journal

Nature Metabolism, 2(4)

ISSN

2522-5812

Authors

van Veen, J Edward
Kammel, Laura G
Bunda, Patricia C
et al.

Publication Date

2020-04-01

DOI

10.1038/s42255-020-0189-6

Peer reviewed

Hypothalamic estrogen receptor alpha establishes a sexually dimorphic regulatory node of energy expenditure

J. Edward van Veen[1,2,7], **Laura G. Kammel**[1,2,3,7], **Patricia C. Bunda**[1], **Michael Shum**[4,5], **Michelle S. Reid**[1], **Megan G. Massa**[1,2,6], **Douglas Arneson**[1], **Jae W. Park**[1], **Zhi Zhang**[1,2], **Alexia M. Joseph**[1], **Haley Hrncir**[1], **Marc Liesa**[4,5], **Arthur P. Arnold**[1,2], **Xia Yang**[1], **Stephanie M. Correa**[1,2]

[1]Department of Integrative Biology and Physiology, University of California, Los Angeles, CA, USA

[2]Laboratory of Neuroendocrinology of the Brain Research Institute, University of California, Los Angeles, CA, USA

[3]Molecular, Cellular, and Integrative Physiology Graduate Program, University of California, Los Angeles, CA, USA

[4]Division of Endocrinology, Department of Medicine, and Department of Molecular and Medical Pharmacology, David Geffen School of Medicine, University of California, Los Angeles, CA, USA

[5]Molecular Biology Institute, University of California, Los Angeles, CA, USA

[6]Neuroscience Interdepartmental Doctoral Program, University of California, Los Angeles, CA, USA

[7]authors contributed equally

Abstract

Estrogen receptor a (ERa) signaling in the ventromedial hypothalamus (VMH) contributes to energy homeostasis by modulating physical activity and thermogenesis. However, the precise neuronal populations involved remain undefined. Here, we describe six neuronal populations in the mouse VMH by using single-cell RNA transcriptomics and in situ hybridization. ERa is enriched in populations showing sex biased expression of reprimo (*Rprm*), tachykinin 1 (*Tac1*), and prodynorphin (*Pdyn*). Female biased expression of *Tac1* and *Rprm* is patterned by ERa-dependent repression during male development, whereas male biased expression of *Pdyn* is maintained by circulating testicular hormone in adulthood. Chemogenetic activation of ERa positive VMH neurons stimulates heat generation and movement in both sexes. However, silencing

---

Rprm gene function increases core temperature selectively in females and ectopic *Rprm* expression in males is associated with reduced core temperature. Together these findings reveal a role for *Rprm* in temperature regulation and ERa in the masculinization of neuron populations that underlie energy expenditure.

Editor Summary:

The ventromedial nucleus of the hypothalamus is known to maintain energy homeostasis by controlling locomotory activity and thermogenesis. Here van Veen, Kammel et al. identified heterogeneous neuronal populations with sexual dimorphic gene expression and functions by using single cell RNA analysis.

Women transitioning to menopause exhibit decreased energy expenditure and decreased fat oxidation compared to age-matched premenopausal women[1]. Similar to humans, rodents exhibit estrogen-induced changes in energy expenditure; female rats exhibit cyclic patterns of wheel running throughout the estrous cycle[2,3] and female mice exhibit similar cyclicity in temperature and locomotion[4–6]. These effects are mediated by estrogen receptor alpha (ERα) signaling: eliminating ERα either globally or in the central nervous system leads to obesity due increased feeding, reduced movement, and reduced thermogenesis[7–9]. In women, estrogen-based hormone therapy can improve metabolic profiles after menopause, but is associated with higher cardiovascular disease risk[10] and, in the case of estrogen plus progestogen therapy, higher breast cancer risk[11]. To ultimately circumvent the risks associated with systemic estrogen therapy, pinpointing the neurons that control systemic energy balance and defining their responses to estrogen signaling is of vital importance.

Recent work has begun to define the neuron populations that mediate the effects of ERα signaling on energy balance. Conditional knockout mouse models suggest that ERα signaling modulates feeding in female mice via neurons of the pro-opiomelanocortin (*Pomc*) lineage, possibly located in the arcuate nucleus (ARC)[5,9,12,13] or outside the medial basal hypothalamus[14–16]. Additionally, ERα signaling modulates two types of energy expenditure, spontaneous physical activity and thermogenesis, via neurons of the steroidogenic factor 1 (*Sf1/Nr5a1*) lineage in the ventromedial hypothalamus (VMH)[9,13,17,18]. However, ERα-expressing neurons of the VMH have many functions. In addition to female-specific roles in energy expenditure, ERα^{+} VMH neurons control fear, territorial aggression, and self-defense in males, maternal aggression in females, and mating behaviors in both sexes[19–24]. We hypothesize that these diverse and sex-specific functions are mediated by distinct subpopulations of ERα^{+} neurons. Consistent with this notion, distinct neuronal ensembles are activated in the ventrolateral region of the VMH (VMHvl) of male mice during interactions with male or female conspecifics[25]. A subset of ERα^{+} neurons in the VMH that likely co-express tachykinin 1 (*Tac1*), oxytocin receptor (*Oxtr*), and melanocortin 4 receptor (*Mc4r*) drive estrogen-dependent changes in physical activity in females[18,26,27]. However, the VMHvl populations that control most other sex-specific functions, such as estrogen-dependent increases in thermogenesis, have not been identified.

The VMH is sexually dimorphic with respect to hormone responsiveness, gene expression, neurochemistry, synaptic organization, and neuron function[28–31]. Here, we use RNA

sequencing with single cell resolution and RNA in situ hybridization (ISH) to test the hypothesis that neurons in this region are heterogeneous and sexually dimorphic. We define six major neuron populations in the VMH and focus on a sexually dimorphic transcript in the VMHvl, reprimo (*Rprm*), which we find regulates core body temperature. Collectively, these studies demonstrate that estrogen regulates energy expenditure in females through two intermingled but distinct neuronal subsets that express *Tac1* or *Rprm* and suggest that the VMH serves as a hormone-responsive nexus of distinct neural circuits controlling metabolic homeostasis.

RESULTS

Single Cell Transcriptomics Reveals Neuronal Heterogeneity in the VMH

We used a fluorescent reporter strategy to isolate neurons of the VMH and single cell RNA sequencing to cluster neurons by similarities in transcriptional signature. To selectively label VMH neurons, the *Sf1^Cre* driver[32] was crossed to mice carrying a latent allele of tdTomato *(Ai14)*[33] (Figure 1a). Importantly, this strategy yields tdTomato expression in neurons of the entire VMH upon Cre expression, including in the ventrolateral VMH where it overlaps with ERα immunoreactivity in both males and females (Figure 1b, c) as in[34]. tdTomato expression in surrounding hypothalamic regions, the dorsomedial hypothalamus (DMH) and the arcuate nucleus (ARC), was detectable but scattered and infrequent (Figure 1b, c, white arrowheads). Fluorescence aided cell sorting (FACS) was performed on single-cell suspensions of hypothalamus to isolate live neurons of the *Sf1* lineage for single cell transcriptomic analysis (Figure 1d, for complete gating strategy see Extended Data Figure 1).

Unicellular transcriptional analysis of 530 single cells from 3 male and 3 female postnatal day (P) 10 mice detected a median of 5890 unique molecular identifiers (UMIs: each corresponding to one unique pre-amplification transcript) and 2556 genes per single cell. Transcriptomic data revealed strong and consistent expression of the neuronal markers β3-tubulin (*Tubb3*) and neurofilament light peptide (*Nefl*), while very few cells exhibited detectable expression of the glial markers *Gfap* and *Olig1* (Figure 2a). Consistent with the VMH being predominantly glutamatergic, high expression of the glutamatergic marker *Slc17a6* and consistently low expression of the GABAergic marker *Slc32a1* was observed in all samples (Figure 2a). Finally, to assess how dissociation and FACS sorting may have affected gene expression, we examined immediate early gene expression. Expression of *Fos* and *Arc*, used as a readout for isolation stress and activation[35,36], appears undetectable in the majority of cells obtained from different animals and sexes (Figure 2a). Overall, we conclude that the *Sf1^Cre*-mediated fluorescent reporter strategy primarily yields live glutamatergic VMH neurons.

To determine if VMH neurons show heterogeneity in gene expression profiles, we used a Shared Nearest Neighbor (SNN) algorithm to identify clusters comprised of transcriptionally similar cells[37,38]. A t-distributed Stochastic Neighbor Embedding (tSNE) visualization of all cells shows a main group of clusters and two divergent clusters (Extended Data Figure 2a). The divergent clusters showed markers indicating a non-neuronal, or non-VMH origin: one marked by differential expression of apolipoprotein E (*Apoe*) and many other markers of

glial-like signature and one marked by differential expression of proopiomelanocortin (*Pomc*) and many other markers indicating an ARC derived origin. For subsequent analyses, we removed these clusters to focus on VMH derived neurons. Within putative VMH neurons, we identified a total of six clusters, hereby identified by the top most differentially expressed transcript within each cluster (Figure 2b): *Tac1*, which has been previously demonstrated to promote physical activity in female mice[18]; reprimo (*Rprm*), a TP53 and ERα regulated gene[39] with no described role in the brain; prodynorphin (*Pdyn*), a gene encoding an endogenous opioid precursor with described roles in leptin-regulated energy homeostasis throughout the hypothalamus[40]; somatostatin (*Sst*), a neuropeptide precursor gene which has hypothalamic roles in the negative regulation of growth hormone axis[41] and feeding[42]; hippocalcin-like protein 1 (*Hpcal1*) encoding a neuron-specific calcium binding protein; and galanin (*Gal*), which encodes a neuropeptide shown to increase food consumption when injected into the VMH of rats[43]. Comparing overall transcriptional signatures among the six VMH clusters (Figure 2d), the most divergent population are neurons expressing *Sst*, with the remaining clusters showing more transcriptional similarity. The expression of cluster-defining markers appears largely mutually exclusive (Figure 2e – for raw values see Source Data Figure 2), suggesting distinct molecular signatures among neuron clusters of the VMH. All the neuron clusters identified in the unicellular analysis of the VMH were obtained by analyzing males and females together as has been done previously when looking for sex differences by single cell RNA sequencing[44–46]. At this stage of development, there were neurons of both male and female origin in each of the identified clusters (Extended Data Figure 2b).

Female Biased Neuronal Ensemble Marker Genes Colocalize with ERα

To test the prediction that each neuronal cluster generated by gene expression would have a correspondingly distinct spatial distribution within the intact VMH, expression of the cluster-defining markers was detected and localized in adult mice using ISH. Further confirming the efficiency of VMH neuron isolation used in the scRNA-seq, expression of all presumptive VMH marker genes was detected within the anatomical boundaries of the VMH (Figure 3a–d, Extended Data Figure 3a,b). Sexually dimorphic expression of *Tac1*, *Rprm*, and *Pdyn* were observed in the VMHvl (Figure 3a–c). Specifically, *Tac1* and *Rprm* expression were both significantly enriched in females within the VMHvl (Figure 3a, b). In contrast, *Pdyn* expression was significantly enriched in males within the VMHvl, although both males and females showed robust expression of *Pdyn* in the dorsomedial VMH (Figure 3c). Finally, we did not detect any major differences in expression of *Sst* between males and females (Figure 3d). Analysis of hypothalamic regions both rostral and caudal to the VMH shows similar expression of *Pdyn*, *Tac1*, and *Sst* among the sexes and only limited expression of *Rprm* (Extended Data Figure 3c). These spatial analyses suggest that the sex differences in *Tac1*, *Rprm*, and *Pdyn* expression are restricted to the VMHvl.

Tac1 and *Rprm* expression are enriched in the female VMHvl. To test the extent to which *Tac1* and *Rprm* co-localize on a cell by cell basis in the VMHvl, we performed two color fluorescent *in situ* hybridization (FISH). Whereas some cells appear to express both *Tac1* and *Rprm*, many cells express either *Rprm* alone or *Tac1* alone (Figure 4a). Among cells expressing either marker, the largest proportions of cells express *Rprm* (58.6%) or *Tac1*

(24.5%) in a mutually exclusive fashion, followed by cells co-expressing *Rprm* and *Tac1* (16.6%) (Figure 4b). Scattered *Sst* expressing cells were also observed in the female VMHvl but did not co-localize with either *Rprm* (Extended Data Figure 4a) or *Tac1* (Extended Data Figure 4b).

To directly test VMHvl expressed markers for co-localization with ERα, we performed dual immuno-FISH (Figure 4c–h, Extended Data Figure 4c). *Tac1* and *Rprm* were frequently co-expressed with ERα in females (Figure 4c,d,i,j), whereas *Pdyn* showed more limited co-expression with ERα, predominantly in males (Figure 4e,k). Considering only cells expressing *Tac1*, co-expression of ERα was prominent in females (from percentages in Figure 4i: 51.0/(51.0+35.7) = 58.8%) but rare in males (12.8%) (Figure 4c,f,i). Considering only cells expressing *Rprm*, co-expression of ERα was prominent in females (70.3%) but not detected in males (0%) (Figure 4d,g,j). In males, immunoreactivity for ERα was weak but detectable in *Pdyn*+ cells (Figure 4e). *Pdyn* was rare in the VMHvl of females (Figure 4h). Considering only cells expressing *Pdyn*, co-expression with ERα was observed in both females (27.5%) and in males (20.4%) (Figure 4k). While *Sst* expression is sparse in the VMHvl of males and females, the majority (75.7%) of *Sst* expressing cells in females do co-express ERα (Extended Data Figure 4c,d) particularly in the most medial portion of the VMHvl, as shown for rats[47].

Organizational Sex Differences in the VMH Are Patterned by Estrogen Signaling

Sex hormones mediate permanent (organizational) differentiating effects on the brain during development, as well as reversible (activational) effects during adulthood, with additional contributions to sex differences caused by sex chromosome encoded genes expressed within brain cells. To delineate how sexually dimorphic expression of cluster markers develops in the VMHvl, we used the four-core genotypes model[48] to dissociate the effects of gonadal sex and sex chromosome complement (Figure 5a). This model reveals effects of sex chromosome complement in comparisons of XX or XY mice with the same gonads and reveals effects of hormones in comparisons of gonadal females or gonadal males with the same sex chromosome complement. Here we distinguish between organizational and activational effects of gonadal hormones using gonadectomized (GDX) and intact mice (Figure 5a).

Expression patterns of both *Tac1* (Figure 5b) and *Rprm* (Figure 5c) were unchanged by GDX in females, showing that hormonal activation is not essential for maintaining sex differences in their expression. Moreover, the number of X or Y chromosomes in gonadal females did not change *Tac1* or *Rprm* expression, suggesting that the sex chromosome complement does not control sexual differentiation of these genes. Instead, gonadal sex was critical for female-biased expression of *Tac1* and *Rprm*, suggesting that these patterns are established during development and maintained in adulthood (Figure 5b, c). In contrast, the expression pattern of *Pdyn* was similar among all groups except gonad-intact males, in which *Pdyn* expression is upregulated in the VMHvl (Extended Data Figure 5a), suggesting that *Pdyn* expression is maintained by differences in testicular sex hormone signaling in adulthood. Finally, we did not observe any sex differences in *Sst* along any of the three phenotypic comparisons (Extended Data Figure 5b).

To directly test if estrogen signaling via ERα is responsible for organizational differences observed in VMH gene expression, we developmentally ablated *Esr1* using *Esr1$^{fl/fl}$;Nkx2–1^{Cre}* mice, which show developmental loss of ERα in the mediobasal hypothalamus[14]. Mice lacking *Esr1* in the VMH display the expected loss of ERα (Figure 5d, f). Female mice lacking ERα exhibit a slight but significant increase in *Tac1* expression (Figure 5d, e) and no change in *Rprm* expression (Figure 5f, g). In contrast, male mice lacking ERα show a much more visually striking phenotype: significant increases in *Tac1* (Figure 5d, e) and *Rprm* (Figure 5f, g) expression, reminiscent of what is seen in wild-type female mice. Together with data obtained from the four core genotypes, our findings suggest a model in which estrogen signaling, mediated by ERα, creates sexual dimorphism in the VMH by permanently repressing expression of *Tac1* and *Rprm* in males.

Chemogenetic Activation of *Esr1$^+$* Neurons Increases Energy Expenditure in Males and Females

Estrogen has long been known to increase neuronal excitability and depolarization in the VMH[49,50], via MAPK activation[51]. Chemogenetic hM3Dq Designer Receptors Exclusively Activated by Designer Drugs (DREADDs) also rapidly increase neuronal excitability and ERK1/2 phosphorylation[52], thereby potentially mimicking the effects of estrogen mediated activation. To test if activation of ERα$^+$ VMHvl neurons can induce movement and heat generation, we bilaterally delivered AAVs encoding DREADDs to the VMHvl of *Esr1^{Cre}* mice by stereotaxic injection (Figure 6a). Both male and female mice show VMHvl-associated expression of the mCherry fluorescent reporter (Figure 6b), indicating successful targeting, transduction, and recombination of the DREADD construct. Further, *Esr1^{Cre}* mice transduced with the DREADD and injected with its ligand, clozapine-N-oxide (CNO), showed cFOS immunoreactivity in the transduced region of the VMHvl (Extended Data Figure 6a,b).

Administration of CNO elicited a sustained increase in heat generation, as measured by indirect calorimetry, in *Esr1^{Cre}* females and males compared to saline administration in the same mice on a different day (Figure 6c). Wild-type littermate animals showed no significant differences in heat production when treated with CNO or saline (Figure 6c). Cross-group comparison of heat production 0.5 h before and 1 h after CNO injection shows *Esr1^{Cre}* males and females exhibit similar increases in heat production (Figure 6d). CNO also elicited a sustained increase in movement, as measured by beam breaks, in *Esr1^{Cre}* females and males compared to saline administration in the same mice on a different day (Figure 6e). Wild-type littermate animals showed no significant differences in movement when treated with CNO or saline (Figure 6e). Cross-group comparison of movement 0.5 h before and 1 h after CNO injection shows *Esr1^{Cre}* males and females exhibit similar significant increases in movement (Figure 6f).

As movement contributes to heat generation, we used infrared imaging of the suprascapular region to assay changes in brown adipose tissue (BAT) activity (Extended Data Figure 6c). CNO-mediated DREADD activation induced a significant increase in temperature of the BAT area 1 hour after CNO injection compared to 10 minutes before injection (Extended Data Figure 6c,d). Saline injections in the same animals on a different day did not induce a

significant change in temperature of the BAT area (Extended Data Figure 6c,d). These data, together with previous studies, demonstrate that *Esr1*$^+$ neurons regulate both movement and temperature.

VMH Expression of *Rprm* Regulates the Sex Specific Central Control of Temperature

To test the hypothesis that the *Rprm*$^+$ subset has selective effects on temperature, we silenced *Rprm* gene function within the VMHvl using cell permeable siRNA pools delivered via bilateral stereotaxic injections (Figure 7a). Stereotaxic coordinates targeting the *Rprm* expressing region of the VMHvl were confirmed by co-injection of AAV-GFP (Figure 7a), and reduction of RPRM protein was confirmed by fluorescent IHC (Figure 7b,c). When compared to animals injected with a non-targeting siRNA, female mice injected with *Rprm* targeting siRNAs showed a significant increase in body temperature (Figure 7d, e). When averaged over 12-hour windows, the increase in temperature was significant in both the active night phase and the inactive day phase (Figure 7e). To test if *Rprm* knockdown affects thermogenesis, we analyzed BAT histology and measured temperature in the suprascapular region using infrared thermography. Female mice in which *Rprm* had been knocked down show a significant increase in intrascapular temperature unaffected by circulating ovarian hormone (Extended Data Figure 7a,b) rather than an effect on heat loss (Extended Data Figure 7c), and a slight decrease in BAT lipid content (Extended Data Figure 7d). Notably, *Rprm* knockdown did not induce changes in physical activity (Figure 7f), suggesting that *Rprm* selectively regulates temperature. Contrasting these results, male mice injected with *Rprm* targeting siRNA pools showed no significant difference in body temperature or movement at any point of the day or night (Figure 7g–i), demonstrating that, in mice, *Rprm* expression regulates core temperature in a sex specific fashion.

Given that developmental loss of ERα in males induces *Rprm* expression in the VMHvl (Figure 5e,g), we next asked if ERα-deficient males show a body temperature phenotype. Compared to littermate male *Esr1*$^{fl/fl}$ mice, male *Esr1*$^{fl/fl}$; *Nkx2–1*^{Cre} mice exhibit decreased core body temperature across two hours at night (Figure 7j,k) and a slight increase in BAT lipid content (Extended Data Figure 7e), further supporting the notion that expression of *Rprm* in the VMHvl decreases core body temperature. Finally, there was no significant effect of *Esr1* knockout on movement in male mice (Figure 7l). These data demonstrate that *Rprm* in the VMHvl functions to alter thermogenesis without affecting physical activity. Together with evidence that *Tac1* neurons selectively regulate movement[18], these findings suggest that there are at least two classes of ERα$^+$ neurons in the VMHvl that are functionally distinct, and together coordinate the female specific effects of this hormone-responsive region.

DISCUSSION

The VMH is one of the brain's longest known sexually dimorphic regions. Gene expression within the VMH, particularly in the VMHvl subdivision, is sexually differentiated by sex hormones during critical developmental periods[27,29,50,51]. In adults, expression of *Esr1* transcript and ERα protein are higher in the VMHvl of females compared to males, and ERα signaling coordinates the increased movement and thermogenesis that accompany the

sexually receptive period in female mice[13,52]. In this study, we used single cell RNA sequencing as the first step in our aim to identify clusters of VMH neurons with sex-specific metabolic functions. Single cell RNA sequencing has led to dramatic advances in our understanding of cellular heterogeneity in the hypothalamus[53,54]. A recently completed single cell census of the VMH identified 40 neuronal sub-types, with 17 found in the VMHvl alone[55]. In contrast, we identified six clusters of neurons that we mapped to the VMH only two of which are restricted to the VMHvl. It is notable that none of the top cluster defining markers (*Tac1, Rprm, Pdyn, Sst, Gal*, and *Hpcal1*) defined here were identified as top cluster defining markers by the higher resolution study[55]. It is likely that our top markers each encompass several of these smaller clusters; indeed when looking more specifically for sex differences the higher resolution analysis similarly identifies *Rprm* and *Pdyn* as female and male biased, respectively. We performed our sequencing on neurons harvested ten days after birth, which has both significant advantages and drawbacks. It revealed populations established in development, before they are altered by hormonal changes associated with experience, puberty, or by the estrous cycle. We note that it is entirely possible that there are very interesting gene expression patterns that only emerge later, which would corroborate work showing that puberty represents a sensitive period for steroid-dependent brain organization[56] and possible effects of social experience on VMHvl neurons[25]. In spite of these important caveats, our extensive validation experiments were done in adults and confirm all of the populations identified by the sequencing analysis. Additionally, *in situ* hybridization comparing the sexes revealed sexually dimorphic populations in the VMHvl that scRNA sequencing did not resolve. The analyses used here identified clusters with differential expression of genes with known functional significance in the VMH (e.g. *Tac1, Sst*) and an assembly of neurons marked by female-biased expression of ERα and *Rprm*, which we show specifically controls core body temperature in a movement-independent manner.

We find that sex hormone signaling during development drives the emergence of two female-specific gene expression signatures in *Esr1*^{+} neurons, defined by largely mutually exclusive expression of either *Tac1* or *Rprm*. We show that these gene expression patterns are developmentally organized by circulating gonadal hormones, and thus do not require continued hormonal signaling for maintenance in adulthood. The *Esr1* knockout studies reported here demonstrate that this is the result of ERα dependent permanent repression of *Tac1* and *Rprm* in males. These findings support the long-held notion that estradiol, as a metabolite of testosterone, plays a major role in the early permanent masculinization of the mammalian brain in males and the expression of male-specific behaviors[57]. These long-term changes in gene expression are mediated by epigenetic modifications, although the exact mechanisms whereby they occur and are maintained remain to be determined[58]. The male-specific gene expression pattern of *Pdyn* is mediated by testicular hormones, in line with previous reports showing that the expression of dynorphin, the neuropeptide encoded by the *Pdyn* gene, is regulated by gonadal hormones in several hypothalamic regions[59]. However, unlike *Tac1* and *Rprm*, the male specific gene expression pattern of *Pdyn* was maintained by sex hormones in adulthood rather than permanently patterned by sex hormones in development. Together these data support the notion that gonadal hormones can induce sex

differences in gene expression within neuron subsets by both permanent (organizational) and transient (activational) mechanisms.

To date, several lines of evidence suggest that the effects of estrogens on energy expenditure are mediated by distinct neuronal populations. For example, ablating ERα signaling in a subset of VMH neurons impairs BAT thermogenesis without affecting physical activity[9], whereas inhibiting the development of a subset of ERα^{+} VMH neurons impairs physical activity without affecting thermogenesis[18]. We now report that silencing *Rprm* expression in the VMHvl selectively increases core temperature without significantly affecting physical activity. This effect only occurred in females, likely due to undetectable *Rprm* expression in the male VMHvl. Corroborating these findings, ectopically inducing *Rprm* expression in males by developmental deletion of ERα decreases core body temperature. The literature describing brain expression of *Rprm* is extremely limited[60]. The RPRM protein is very small, comprised of 109 amino acids, and the only predicted domain is a putative transmembrane helix. In human tissues, *Rprm* is expressed at the highest levels in the cervix, uterus, and pituitary[61], all of which are estrogen-responsive tissues. In several breast cancer cell lines, estrogen treatment rapidly represses *Rprm* transcription and this effect is dependent upon ERα, HDAC7, and FOXA1[39]. The effects of estrogen signaling on BAT thermogenesis are partially dependent on inhibition of AMP-kinase (AMPK) that leads to activation of the sympathetic nervous system[13]. Our studies reveal that modulation of *Rprm* expression on thermogenesis may be mediated in part through the BAT. As the function of *Rprm* is likely different in post-mitotic neurons than in dividing cells, a full characterization of neuronal RPRM function will require biochemical purification of RPRM-containing complexes and complete conditional knockout of the *Rprm* gene in future studies.

Functional dissection of sex differences in the neural circuits that control food intake and energy expenditure is critical to understanding the biological basis of sex and gender differences in the control of body weight. Entry into menopause is associated with significant increases in visceral abdominal fat and body weight, without an increase in caloric intake. Instead, adiposity correlates with a decrease in overall energy expenditure, which manifests most strikingly during sleep[1]. Thus, factors that contribute to decreased energy expenditure, such as dysregulated thermogenesis, could be primary risk factors for post-menopausal obesity. As such, the molecular mechanism whereby ERα signaling in *Tac1*^{+} and *Rprm*^{+} neurons drives changes in physical activity or thermogenesis will be of interest for the potential treatment of post-menopausal obesity. Together, our studies suggest a model in which estrogens act on the VMH in a bifunctional and temporally separated manner. During development, estrogen signaling via ERα first permanently masculinizes the VMH, repressing expression of *Tac1* and *Rprm* in males. Later, in adulthood, we predict that estrogen signaling activates *Tac1* and *Rprm* neuron clusters in females to increase energy expenditure. We speculate that *Tac1*^{+} and *Rprm*^{+} neurons are important nodes in the dysregulation of energy expenditure accompanying the abrupt decline in circulating sex hormones experienced during menopause.

Methods

Mice

All studies were carried out in accordance with the recommendations in the Guide for the Care and Use of Laboratory Animals of the National Institutes of Health. UCLA is AALAS accredited and the UCLA Institutional Animal Care and Use Committee (IACUC) approved all animal procedures. Mice expressing the $Sf1^{Cre}$ driver transgene (*Tg(Nr5a1-cre)7Lowl*), the $Nkx2–1^{Cre}$ driver transgene (*Tg(Nkx2–1-cre)2Sand*), and the *Ai14*-tdTomato reporter with loxP-flanked STOP cassette (*Gt(ROSA)26Sort^{tm14(CAG-tdTomato)Hze}*) were maintained on a C57BL/6 genetic background. The *Esr1 floxed* allele (*Esr1^{tm1Sakh}*) was maintained on a CD-1;129P2 mixed background. Breeder male "Four Core Genotypes" mice (FCG, background C57BL/6J) possess a Y chromosome deleted for the testis-determining gene *Sry*, and an *Sry* transgene inserted into chromosome 3. The four genotypes include XX and XY gonadal males (XXM and XYM), and XX and XY gonadal females (XXF and XYF). Genotypes were discriminated using genomic PCR as described in[62]. All other experiments were carried out on C57BL/6J mice (JAX 000664). Except for gonadectomy studies, all experiments were performed in intact males and intact cycling females.

scRNA sequencing

We labeled all VMH neurons by crossing the Cre-dependent tdTomato reporter (*Ai14*)[33] to the $Sf1^{Cre}$ driver[32] to generate $Ai14^{f/f};Sf1^{Cre}$ mice. Because the tdTomato signal is largely restricted to the VMH, a fairly large hypothalamic region was collected under fluorescent illumination. Cells were dissociated using a papain-based enzymatic process (Worthington Biochemical). VMH neurons were sorted by FACS using parameters that select for tdTomato signal. Because tdTomato is expressed in processes and projections, we enriched for cell bodies using a nuclear DNA dye (cell permeant DRAQ5, ThermoFisher). Dead cells were excluded by eliminating cells stained by NucBlue (cell impermeant DAPI). Doublet discrimination was used to ensure single cells were deposited into each well. Individual tdTomato⁺ neurons were sorted into each well of a 96-well plate (Precise WTA kits, BD). The Precise WTA single cell sequencing kits include a well index to identify each cell and a unique molecular identifier (UMI) to identify each transcript and reduce bias due to PCR amplification. Libraries were prepared according to manufacturer's instructions and sequenced on an Illumina NextSeq 500 using paired end 2×75 bp mode giving an average depth of 3×10^5 reads per single cell.

Expression data were analyzed using the R package Seurat[63]. Normalized data were scaled with a linear regression model based on number of UMIs per cell and percentage of reads from the mitochondrial genome to remove unwanted sources of variability and to normalize gene expression data. Analyses included all genes expressed in ≥2 cells, and all cells expressing ≥500 genes and a fraction of mitochondrial reads < 0.17. To cluster cells based on transcriptome similarity, we used Shared Nearest Neighbor (SNN) algorithm[37,38]. For each cell cluster, marker genes were determined by comparing expression in the given cluster against all other clusters using the smart local moving algorithm to iteratively group clusters together[64]. For all differentially expressed gene marker analyses, statistical significance testing was performed with the Seurat default Wilcoxon rank-sum based test

and Benjamini-Hochberg method for multiple testing correction. Genes meeting and adjusted p-value cutoff of less than .05 were considered marker genes. Marker genes were then ranked by the log fold change in relative expression within the cluster, compared to all other clusters.

Mouse Procedures

Mice were anaesthetized with isofluorane and received analgesics (0.01mg/mL buprenorphine, 0.58mg/mL carprofen) pre- and post- surgery. Bilateral ovariectomy and castration surgery with complete removal of the ovaries or the testes was performed on adult mice. For Figure 4, sham or gonadectomized control mice (XXF and XYM) and gonadectomized FCG mice from separate experimental batches are shown together. The Cre-dependent AAV8-hM3Dq-mCherry DREADD (Addgene, titer 4×10^{12} vg/mL, 200 nL to each side) was injected bilaterally into the VMHvl of adult female mice (coordinates: A-P: −1.56 mm from Bregma; lateral: ±0.85 mm from Bregma; D-V: 5.6 mm from the cortex). After 2 weeks of recovery, mice received i.p. injections of CNO (0.3 mg/kg) or vehicle (saline, 0.15% DMSO) 3 hr after the onset of the light phase. Saline and CNO were administered on consecutive days in a randomized balanced design. siRNA pools against *Rprm* or non-targeting controls (Dharmacon, 0.4 mM, 350 nL to each side) were delivered to the VMHvl as described above. Indirect calorimetry was performed in Oxymax metabolic chambers (Columbus Instruments) at room temperature. Gross movement and core body temperature were measured using an IP-implanted G2 eMitter and VitalView software (Starr Life Sciences).

RNA probe generation

Digoxigenin (DIG)- or fluorescein (FITC)-labeled sense and antisense riboprobes for somatostatin (*Sst*), reprimo (*Rprm)*, tachykinin 1 (*Tac1)*, prodynorphin (*Pdyn)*, necdin (*Ndn)*, and proto-oncogene, serine/threonine kinase A-Raf (*Araf)* were in vitro transcribed from template cDNA using T7/T3/SP6 RNA polymerase (DIG/FITC RNA labeling kit, Roche) and purified with RNA Clean & Concentrator (Zymo Research). For template cDNA generation, PCR products for individual genes were amplified from a hypothalamic cDNA library and cloned into pCR 2.1-TOPO or pCR II-TOPO (Invitrogen) for all probes except *Tac1*, which was previously described. Plasmid DNA was isolated from bacterial cultures using ZymoPURE II Plasmid Midiprep kit (Zymo Research), linearized by restriction digest, and purified with DNA Clean & Concentrator (Zymo Research). All PCR products, except *Araf*, were generated using reference primer sequences from the Allen Brain Institute. For *Araf*, cDNA was generated from bases 639–942 (NM_009703.2).

In situ hybridization and immunostaining

The in situ hybridization (ISH) and immunostaining protocols were partially adapted from previously published methods[18]. 18μm-thick cryosections containing the VMH were obtained from paraformaldehyde-fixed mouse brains. Day 1: Upon defrosting to room temperature (rt), slides were washed in PBS, postfixed in 4% PFA, and washed again. TSA-fluorescent ISH (FISH) slides were also incubated in 3% H_2O_2 for 30min to quench endogenous peroxidase activity. To permeabilize the tissues, slides were incubated in proteinase K (1ug/mL) for TSA-FISH and chromogenic ISH (CISH), or 0.3% Triton X-100

in PBS for combined FISH-IHC. CISH slides were postfixed again in 4% PFA for 5 min. Slides were incubated in hyb solution containing probe overnight at 65C. Day 2: Coverslips were removed in solution containing 5x SSC heated to 65C. Slides were then subject to a series of stringency washes, then blocked in NTT containing 2% blocking reagent and HISS for 2 h at rt. Slides were incubated in antibody solution containing either anti-DIG-AP (Millipore-Sigma, cat. 11093274910, dilution 1:5,000), anti-FITC-AP (Millipore-Sigma, cat. 11426338910, dilution 1:5,000), or anti-DIG-POD (Millipore-Sigma, cat. 11207733910, dilution 1:4,000) in 4C overnight. FISH-IHC slides were additionally incubated in anti-ERα (Millipore Sigma, 1:1000). Day 3: Slides were washed in NTT, then NTTML (0.15M NaCl, 0.1M Tris pH 9.5, 50mM $MgCl_2$, 2mM levamisole, and 0.1% Tween-20) to quench endogenous phosphatase activity. Slides were developed in INT/BCIP solution (Roche). FISH-IHC slides were blocked in 10% normal goat serum for 1hr at rt, and incubated with anti-rabbit 647 for 2 h at rt, and incubated in HNPP/Fast red working solution according to manufacturer's instructions (HNPP Fluorescent Detection Set, Roche). To stop the reaction, the slides were washed in PBS, counterstained with DAPI, and immediately stored in −20C to prevent HNPP/Fastred diffusion. TSA-FISH slides were incubated in working solution containing Cy5 Plus tyramide according to manufacturer's instructions (Perkin Elmer). Slides were then washed in NTT and incubated in 3% H_2O_2 for 30min to quench the first tyramide reaction. Slides were then washed in NTT, blocked in in NTT containing 2% blocking reagent and HISS for 2 h at rt, and incubated overnight in anti-FITC-POD (Millipore-Sigma, cat. 11426346910, dilution 1:4,000). Day 4: TSA-FISH slides were washed in NTT, and incubated in working solution containing FITC Plus tyramide according to manufacturer's instructions (Perkin Elmer). The reaction was terminated with NTT and slides were counterstained in DAPI. Control experiments using sense riboprobes and no probes showed negligible signal. Additionally, performing the TSA reaction following 3% H_2O_2 for 30min in the absence of a second POD incubation confirmed adequate quenching. Probes with weaker signal intensity were developed first in TSA-FISH. Additional antibodies used for immunostaining include goat anti-rabbit IgG (H+L), Alexa Fluor 488 (Invitrogen, cat. A11034, Lot 1937195, dilution 1:500); Alexa Fluor 647 goat anti-rabbit (Jackson ImmunoResearch Inc., cat. 111-606-003, dilution 1:500), Rabbit anti-RPRM antibody [N1C3] (Genetex cat. GTX110976, dilution 1:100); mouse anti-GFP [B-2] (Santa Cruz Biotech., cat. sc-9996, dilution 1:50); Rabbit anti-cFos (Synaptic Systems, cat. 226003, dilution 1:200); Rabbit anti-estrogen receptor alpha (Millipore-Sigma, cat. 06–935, dilution 1:1000); and Alexa Fluor 594 goat anti-rabbit (Invitrogen, cat. A11012, dilution 1:500). To achieve adequate signal for anti-RPRM immunohistochemistry, tissues were incubated with primary antibody for 3 days in 4C.

BAT Histology

Brown adipose tissue (BAT) was dissected from the interscapular region and fixed overnight in 4% PFA. 4 μm-thick cryosections were prepared and stained with H&E by the UCLA Translational Pathology Core Laboratory.

Thermogenic Image Analysis—Infrared images were obtained using the e60bx thermogenic camera (FLIR Systems) and analyzed using the FLIR Tools software. All images were obtained at a constant distance to subject in awake animals. The interscapular

region of interest (ROI) was defined as a spherical area located a constant distance from the base of the ears and centered on the scapulae. The tail ROI was defined as a line located at a constant distance starting from the base of the tail. ROI criteria were adapted from[65].

Image Acquisition and Quantification

CISH and BAT histology experiments were with imaged in brightfield on a DM1000 LED microscope (Leica) using 5X or 10X objectives. Semi-quantitative optical density (O.D.) measurements of mRNA in CISH slides were obtained with ImageJ (NIH) following calibration with a calibrated step tablet (Kodak), according to standard protocols[66]. Measurements from the left and right VMH were averaged to calculate the mean O.D. for each animal using predetermined ROIs based on the Franklin and Paxinos Mouse Brain Atlas. Sex differences in O.D. between the caudal VMH and caudal VMHvl were determined by two-way ANOVA with Bonferroni multiple-comparison correction. FISH and IHC experiments were imaged on a LSM780 confocal microscope (Zeiss) using 10X or 20X objectives. Tile-scanned images were stitched using Zen Black (Zeiss). All images were taken with the same z-sampling interval for a given objective and z-stacks were merged to obtain maximum intensity projections. Cyan/magenta/yellow pseudo-colors were applied to all fluorescent images for accessibility. Image processing, limited to brightness and contrast, was performed using the Leica Application Suite (Leica), Zen Black (Zeiss), ImageJ (NIH), and Photoshop (Adobe). Quantification of FISH and immuno-FISH images was done with a custom CellProfiler[67] pipeline designed to define neuronal cell bodies as a 2 pixel width ring around DAPI stained nuclei (pipeline supplied as Supplementary Software 1). All CellProfiler quantification was done on unmanipulated individual confocal images. Median intensity measurements were not subject to any additional filtering or outlier replacement. Statistics and graphing of CellProfiler based quantification were all performed in R studio using a custom R script. To define "positive" versus "negative" staining for any marker of interest dashed lines were drawn based on a normal distribution as follows: in females, roughly 50% of cells appear positive for ERα based on inspection of images and quantifications, so any cells expressing higher than the mean value is counted as positive; *Rprm* cutoff = mean + .5SD (standard deviations); *Tac1* cutoff = mean; *Sst* cutoff = mean + 1.5SD; *Pdyn* cutoff = mean. To test significance of CellProfiler based data, data were first aggregated by animal using mean of median intensity values, such that each animal represents an independent replicate. Aggregated values were first tested for normality using the Shapiro-Wilk method with alpha = .05. All tested datasets fit the normal distribution, and so t-tests were used for each variable analyzed. ISH images in Extended Data figure 3a and Extended Data figure 3b were downloaded from the Allen Mouse Brain Atlas[68].

Data Availability

The data that support the findings of this study are available from the corresponding author upon request and the Reporting Summary is available from the Nature Metabolism website. The single-cell RNA-seq data has been deposited in the NCBI Gene Expression Omnibus under accession number GSE143818. Cellprofiler pipeline used to quantify fluorescent images and source data for Figure 2e are available from the Nature Metabolism website.

Code Availability

Custom R scripts written for single cell analyses and for FISH quantification, statistics, and plotting available at https://github.com/jevanveen/vanveenkammel.
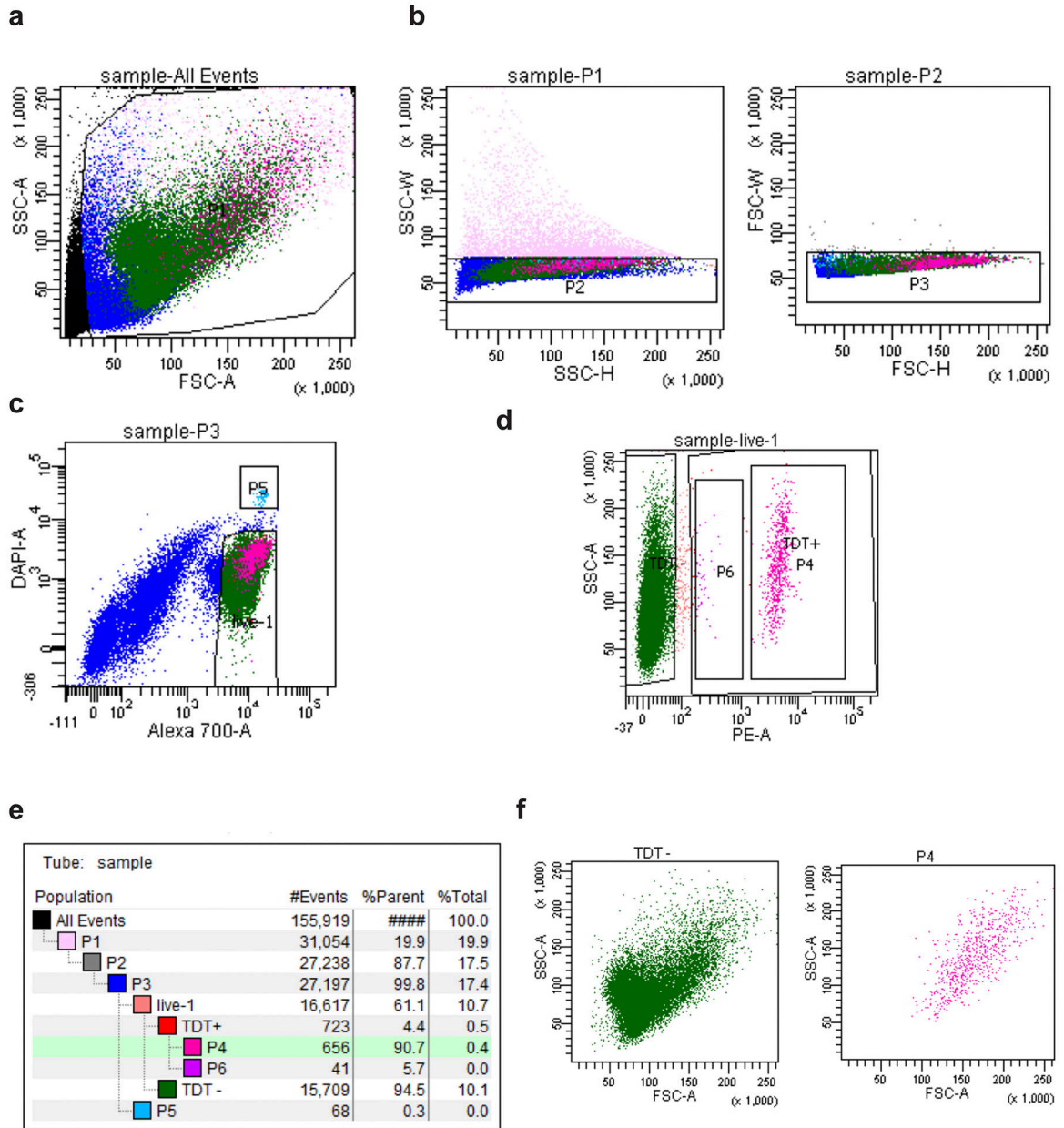
Extended Data

Extended Data Fig. 1. FACS strategy for the isolation of *Sf1* lineage cells. Related to Figure 1.
a, Gating of all events using forward scatter area (FSC-A) and side scatter area (SSC-A) to select for probable cellular objects (gate p1) based on size and internal complexity. **b,** FSC and SSC gating to remove doublets (gate p2,p3). **c,** Gating using live cell permeable (Alexa 700,DRAQ5) and live cell impermeable (DAPI) DNA dyes. Objects displaying high DRAQ5 and low DAPI are nucleated and alive (gate live-1). **d,** Gating to select nucleated single cells displaying red fluorescence (gate p4). TdTomato+ cells were sorted into 96 well plates for downstream scRNA-Seq. **e,** Hierarchy of populations demonstrating that tdTomato+ (p4) cells comprise ~4% of all live, nucleated objects obtained from rough dissection and dissociation of hypothalami. **f,** graphs comparing FSC-A and SSC-A of live, nucleated

tdTomato- objects to live, nucleated tdTomato+ objects. FACS plots are representative of two separate experiments comprised of n = 3 female mice and n = 3 male mice.
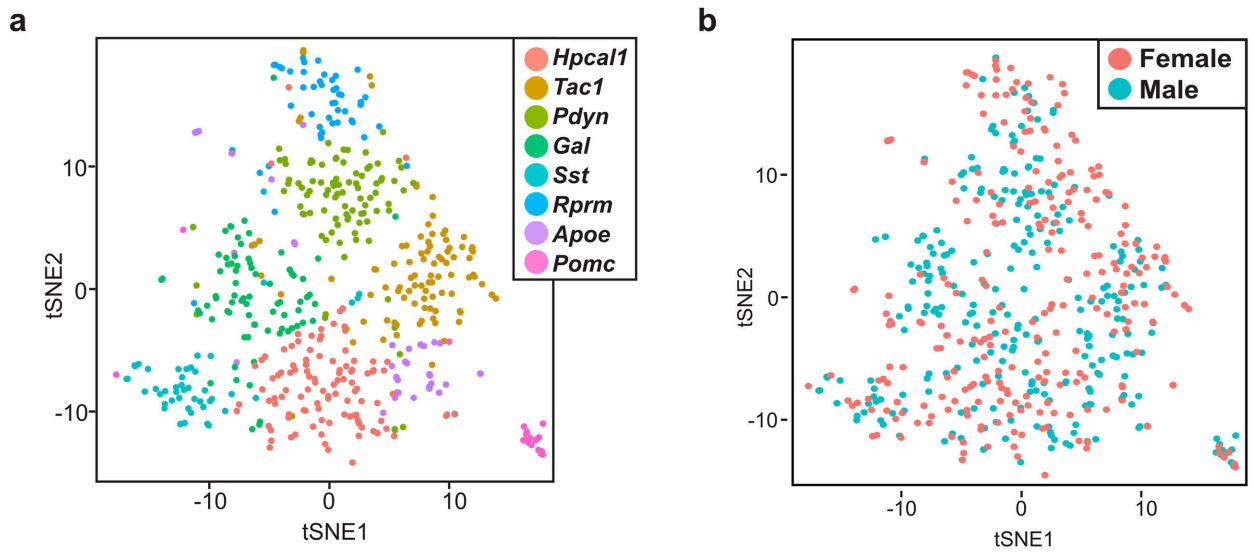
Extended Data Fig. 2. The transcriptional architecture of the VMH is similar in males and females. Related to Figure 2.
a, tSNE showing all clusters identified by bioinformatic analyses including those predicted to be from the arcuate nucleus of the hypothalamus (*Pomc*) and rare non-neuronal cells (*Apoe*) **b,** tSNE showing that male and female neurons are present in all clusters identified.
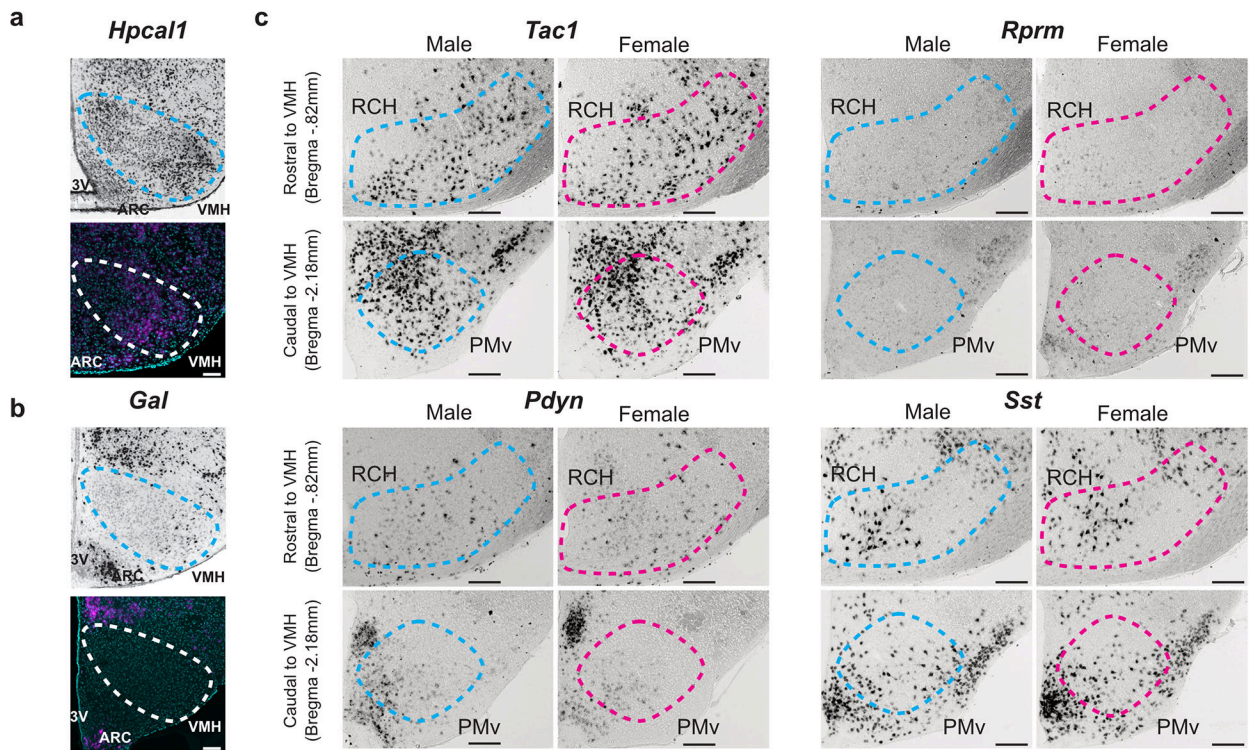
Extended Data Fig. 3. Clustering and expression of broadly expressed VMH markers and markers outside of the VMH Related to Figure 3.

a, *Hpcal1* expression appears diffusely in the adult male (image from Allen Brain Atlas), *top*, and female VMH, *below* (representative of images from n = 5 mice). **b,** *Gal* expression is restricted to scattered cells in the adult male (image from Allen Brain Atlas), *top*, and female VMH, *below* (representative of images from n = 1 mouse). **c,** expression of *Tac1*, *Rprm*, *Pdyn*, and *Sst* in the retrochiasmatic area (RCH) and ventral premammillary nucleus (PMv), adjacent to the VMH along the rostral-caudal axis in males (n = 3 mice) and females (n = 4 mice). Scalebars = 100μm, DAPI shown in cyan.
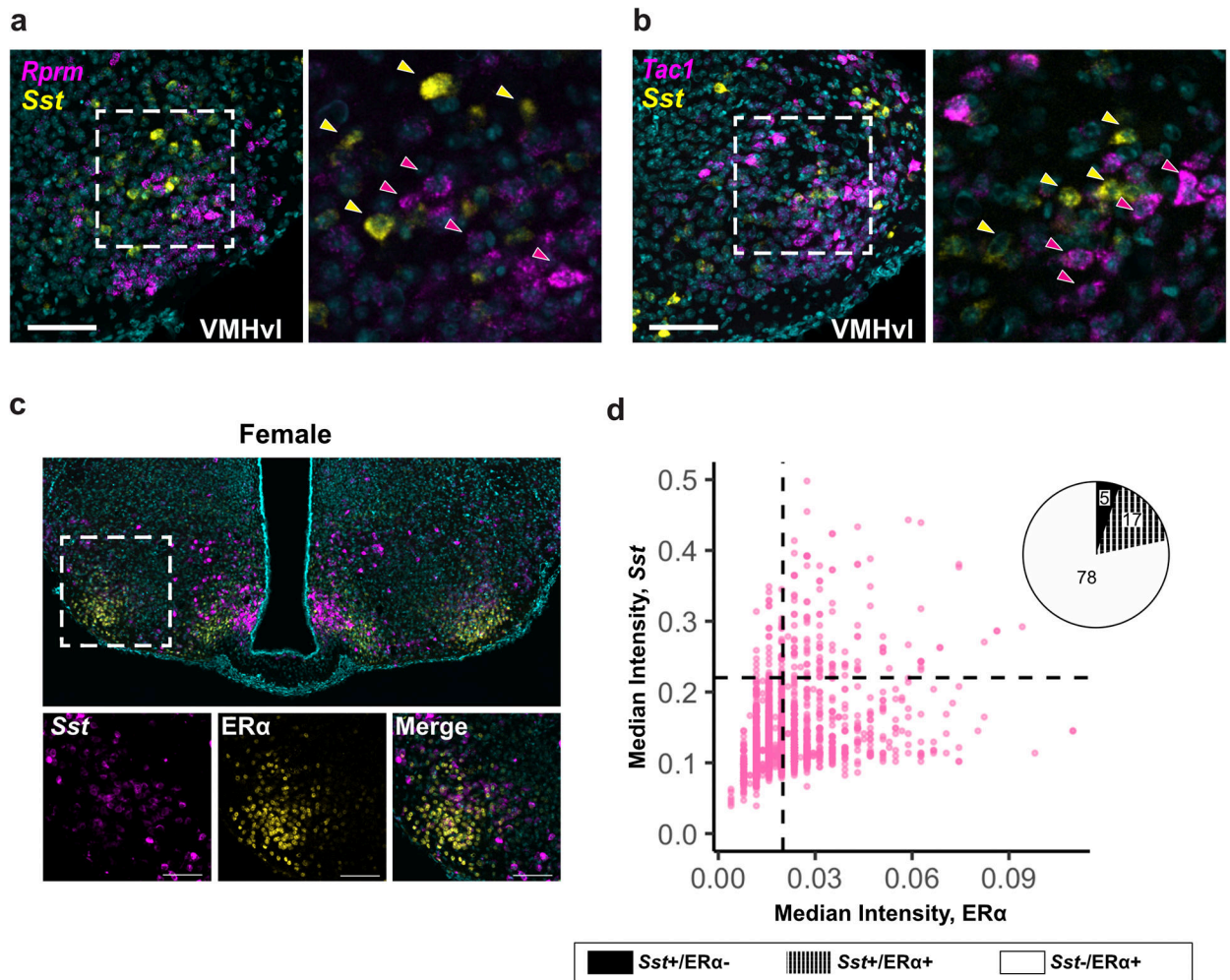
Extended Data Fig. 4. Limited overlap in expression of *Sst* with *Tac1* or *Rprm*. Related to Figure 4.
a, *Sst* (yellow) and *Rprm* (magenta) transcripts in the VMHvl (images representative of n = 5 female mice). **b,** *Sst* (yellow) and *Tac1* (magenta) transcripts in the VMHvl (images representative of n = 5 female mice). **c,** *Sst* transcripts are sparse but often associated with ERα expression (images representative of n = 6 female mice). **d,** quantification of *Sst* transcripts and ERα immunoreactivity confirms that while the majority of ERα expressing cells do not co-express *Sst*, the majority of *Sst* expressing cells co-express ERα (n = 6 female mice).
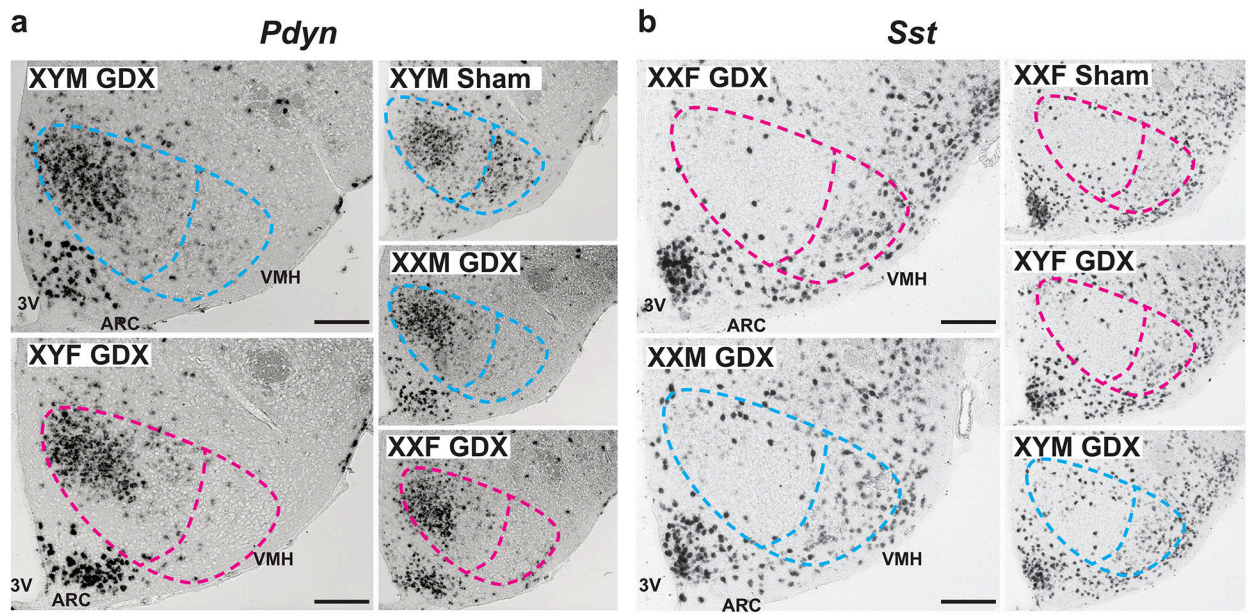
Extended Data Fig. 5. Activational effects of hormones maintain male-biased expression of *Pdyn*. Related to Figure 5.

a, four core genotypes of mice (n = 2 animals for all GDX panels, n = 3 animals for sham panel) analysis showing that *Pdyn* expression is maintained in adult males by circulating testicular hormone. **b,** four core genotypes analysis confirming that there is no sex difference in *Sst* expression(n = 2 animals for all GDX panels, n = 3 animals for sham panel). Dashed line shows boundary of VMH and VMHvl, in blue for male and magenta for female. Scalebars = 200μm.
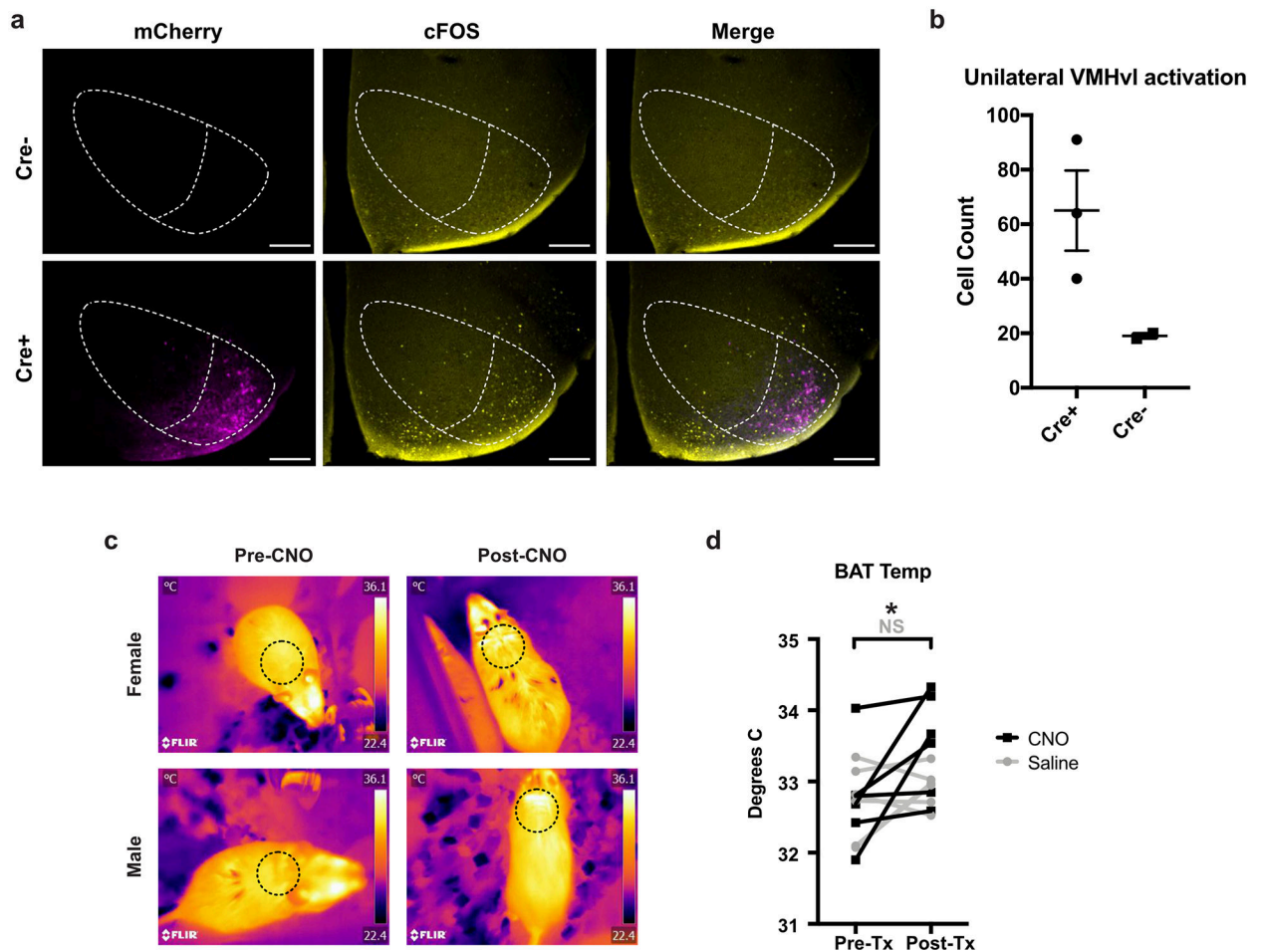
Extended Data Fig. 6. Chemogenetic activation of *Esr1*$^+$ VMHvl neurons enhances BAT thermogenesis.
cFOS immunoreactivity in wild-type (*Esr1*^{Cre}-negative, n = 2 animals) or *Esr1*^{Cre} (*Esr1*^{Cre}-positive, n = 3 animals) littermate female mice perfused 90 minutes after CNO injection. Scalebar = 200 μm. **b,** Image quantification, mean±SEM shown. **c,** Infrared thermography of male and female *Esr1*^{Cre} mice (n = 6: 4 male mice + 2 female mice) injected with AAV-DIO-hM3Dq-mCherry, 30 minutes before (Pre-Tx) and 60 minutes after injection with CNO or saline (Post-Tx). Dashed line indicates interscapular region directly above BAT. **d,** quantification of shows a rise in intrascapular temperature following treatment with CNO compared to saline treatment in the same animals on a different day. Two-way RM ANOVA: *pre vs post: F(1,10) = 6.331, p = .0306. Sidak's multiple comparisons test: pre vs post CNO: t = 2.763, p = .0397; pre vs post saline: t = .7954, p = .6918.*
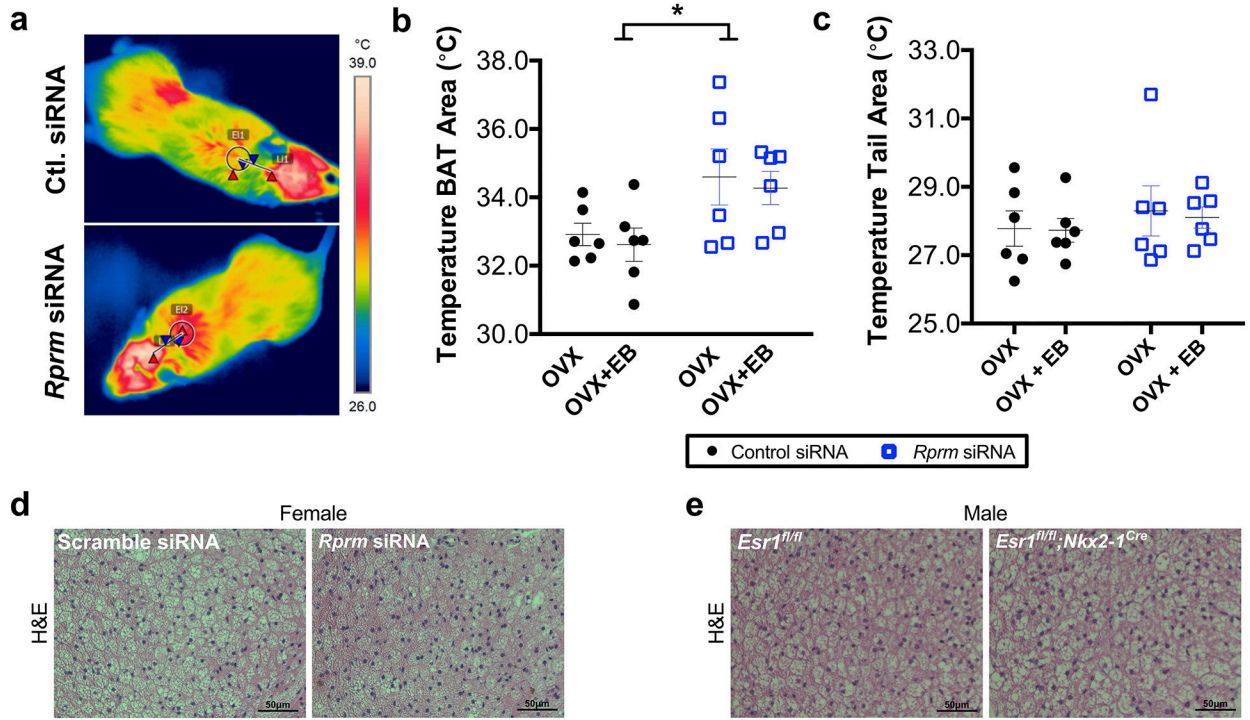
Extended Data Fig. 7. Depletion of *Rprm* in the VMH enhances BAT thermogenesis.
Representative thermal images of female mice injected with either *Rprm* targeting or non-targeting siRNA pools. **b,** Quantification of thermography shows a significant increase in skin temperature above the interscapular BAT depots in ovariectomized (OVX) female mice injected with *Rprm* targeting siRNA pools (n = 6 animals) compared to OVX female mice injected with non-targeting siRNA pools (n = 6 animals) (Two-way RM ANOVA: *siRNA type ($F_{(1,5)}$ = 16.16, p= 0.0101); hormone treatment ($F_{(1,5)}$ = 0.2471, p = 0.6402); interaction ($F_{(1,5)}$ = 0.0005832, p = 0.9817)*. The effect of *Rprm* depletion on BAT is not changed by estrogen replacement (mean±SEM shown). **c,** Quantification of thermography shows no significant difference in tail skin temperature in ovariectomized (OVX) female mice injected with *Rprm* targeting siRNA pools (n = 6 animals) compared to OVX female mice injected with non-targeting siRNA pools (n = 6 animals) (mean±SEM shown). **d,** representative images of BAT histology showing a slight decrease in lipid content in female mice injected with *Rprm* targeting siRNA pools (n = 8 animals) as compared to female mice injected with non-targeting siRNAs (n = 8 animals). BAT was collected 14 days after siRNA injection. **e,** Representative images of BAT histology in male mice with developmental ablation of hypothalamic ERα (*Esr1^fl/fl; Nkx2–1^Cre*, n = 5 animals) or littermate controls (*Esr1^fl/fl*, n = 5 animals). Scalebars = 50μm.

Supplementary Material

Refer to Web version on PubMed Central for supplementary material.

Acknowledgements

REFERENCES

1. Lovejoy JC, Champagne CM, de Jonge L, Xie H & Smith SR Increased visceral fat and decreased energy expenditure during the menopausal transition. Int J Obes (Lond) 32, 949–58 (2008). [PubMed: 18332882]

2. Slonaker JR The effect of copulation, pregnancy, pseudopregnancy and lactation on the voluntary activity and food consumption of the albino rat. Am J Physiol 71, (1925).

3. Brobeck JR, Wheatland M & Strominger JL Variations in regulation of energy exchange associated with estrus, diestrus and pseudopregnancy in rats. Endocrinology 40, 65–72 (1947). [PubMed: 20286603]

4. Kopp C, Ressel V, Wigger E & Tobler I Influence of estrus cycle and ageing on activity patterns in two inbred mouse strains. Behavioural brain research 167, 165–74 (2006). [PubMed: 16214232]

5. Olofsson LE, Pierce AA & Xu AW Functional requirement of AgRP and NPY neurons in ovarian cycle-dependent regulation of food intake. Proceedings of the National Academy of Sciences of the United States of America 106, 15932–7 (2009). [PubMed: 19805233]

6. Sanchez-Alavez M, Alboni S & Conti B Sex- and age-specific differences in core body temperature of C57Bl/6 mice. Age (Dordr) 33, 89–99 (2011). [PubMed: 20635153]

7. Heine PA, Taylor JA, Iwamoto GA, Lubahn DB & Cooke PS Increased adipose tissue in male and female estrogen receptor-alpha knockout mice. Proceedings of the National Academy of Sciences of the United States of America 97, 12729–34 (2000). [PubMed: 11070086]

8. Park CJ et al. Genetic rescue of nonclassical ERalpha signaling normalizes energy balance in obese Eralpha-null mutant mice. The Journal of clinical investigation 121, 604–12 (2011). [PubMed: 21245576]

9. Xu Y et al. Distinct hypothalamic neurons mediate estrogenic effects on energy homeostasis and reproduction. Cell metabolism 14, 453–65 (2011). [PubMed: 21982706]

10. Hulley S et al. Randomized Trial of Estrogen Plus Progestin for Secondary Prevention of Coronary Heart Disease in Postmenopausal Women. JAMA 280, 605–613 (1998). [PubMed: 9718051]

11. Writing Group for the Women's Health Initiative Investigators. Risks and Benefits of Estrogen Plus Progestin in Healthy Postmenopausal WomenPrincipal Results From the Women's Health Initiative Randomized Controlled Trial. JAMA 288, 321–333 (2002). [PubMed: 12117397]

12. Smith AW, Bosch MA, Wagner EJ, Rønnekleiv OK & Kelly MJ The membrane estrogen receptor ligand STX rapidly enhances GABAergic signaling in NPY/AgRP neurons: role in mediating the anorexigenic effects of 17β-estradiol. American Journal of Physiology-Endocrinology and Metabolism 305, E632–E640 (2013).

13. Martinez de Morentin PB et al. Estradiol Regulates Brown Adipose Tissue Thermogenesis via Hypothalamic AMPK. Cell metabolism 20, 41–53 (2014). [PubMed: 24856932]

14. Herber CB et al. Estrogen signaling in arcuate Kiss1 neurons suppresses a sex-dependent female circuit promoting dense strong bones. Nature Communications 10, 163 (2019).

15. Asarian L & Geary N Sex differences in the physiology of eating. American Journal of Physiology-Regulatory, Integrative and Comparative Physiology 305, R1215–R1267 (2013).

16. Rivera HM & Stincic TL Estradiol and the control of feeding behavior. Steroids 133, 44–52 (2018). [PubMed: 29180290]

17. Musatov S et al. Silencing of estrogen receptor alpha in the ventromedial nucleus of hypothalamus leads to metabolic syndrome. Proceedings of the National Academy of Sciences of the United States of America 104, 2501–6 (2007). [PubMed: 17284595]

18. Correa SM et al. An estrogen-responsive module in the ventromedial hypothalamus selectively drives sex-specific activity in females. Cell Rep 10, 62–74 (2015). [PubMed: 25543145]

19. Hashikawa K et al. Esr1+ cells in the ventromedial hypothalamus control female aggression. Nature Neuroscience 20, 1580 (2017). [PubMed: 28920934]

20. Lin D et al. Functional identification of an aggression locus in the mouse hypothalamus. Nature 470, 221–6 (2011). [PubMed: 21307935]

21. Lee H et al. Scalable control of mounting and attack by Esr1+ neurons in the ventromedial hypothalamus. Nature 509, 627–32 (2014). [PubMed: 24739975]

22. Yang CF et al. Sexually dimorphic neurons in the ventromedial hypothalamus govern mating in both sexes and aggression in males. Cell 153, 896–909 (2013). [PubMed: 23663785]

23. Wang L et al. Hypothalamic Control of Conspecific Self-Defense. Cell Reports 26, 1747–1758.e5 (2019). [PubMed: 30759387]

24. Silva BA et al. Independent hypothalamic circuits for social and predator fear. Nature neuroscience 16, 1731–3 (2013). [PubMed: 24212674]

25. Remedios R et al. Social behaviour shapes hypothalamic neural ensemble representations of conspecific sex. Nature 550, 388–392 (2017). [PubMed: 29052632]

26. Narita K, Murata T & Matsuoka S The ventromedial hypothalamus oxytocin induces locomotor behavior regulated by estrogen. Physiology & behavior 164, 107–12 (2016). [PubMed: 27237044]

27. Krause WC et al. Estrogen Drives Melanocortin Neurons To Reduce Sedentary Behavior. bioRxiv 794792 (2019) doi:10.1101/794792.

28. Flanagan-Cato LM Sex differences in the neural circuit that mediates female sexual receptivity. Frontiers in neuroendocrinology 32, 124–36 (2011). [PubMed: 21338620]

29. Yang T & Shah NM Molecular and neural control of sexually dimorphic social behaviors. Curr Opin Neurobiol 38, 89–95 (2016). [PubMed: 27162162]

30. Krause WC & Ingraham HA Origins and Functions of the Ventrolateral VMH: A Complex Neuronal Cluster Orchestrating Sex Differences in Metabolism and Behavior in Sex and Gender Factors Affecting Metabolic Homeostasis, Diabetes and Obesity (ed. Mauvais Jarvis, F.) 199–213 (Springer International Publishing, 2017). doi:10.1007/978-3-319-70178-3_10.

31. Kammel LG & Correa SM Selective sexual differentiation of neurone populations may contribute to sex-specific outputs of the ventromedial nucleus of the hypothalamus. Journal of Neuroendocrinology n/a, e12801 (2019). [PubMed: 31605642]

32. Dhillon H et al. Leptin directly activates SF1 neurons in the VMH, and this action by leptin is required for normal body-weight homeostasis. Neuron 49, 191–203 (2006). [PubMed: 16423694]

33. Madisen L et al. A robust and high-throughput Cre reporting and characterization system for the whole mouse brain. Nature neuroscience 13, 133–40 (2010). [PubMed: 20023653]

34. Cheung CC, Kurrasch DM, Liang JK & Ingraham HA Genetic labeling of steroidogenic factor-1 (SF-1) neurons in mice reveals ventromedial nucleus of the hypothalamus (VMH) circuitry beginning at neurogenesis and development of a separate non-SF-1 neuronal cluster in the ventrolateral VMH. J Comp Neurol 521, 1268–88 (2012).

35. Sheng M & Greenberg ME The regulation and function of c-fos and other immediate early genes in the nervous system. Neuron 4, 477–485 (1990). [PubMed: 1969743]

36. Wu YE, Pan L, Zuo Y, Li X & Hong W Detecting Activated Cell Populations Using Single-Cell RNA-Seq. Neuron 96, 313–329.e6 (2017). [PubMed: 29024657]

37. Van der Maaten LJP & Hinton GE Visualizing high-dimensional data using t-SNE. J. Mach. Learn. Res 9, 2579–2605 (2008).

38. Mwangi B, Soares JC & Hasan KM Visualization and unsupervised predictive clustering of high-dimensional multimodal neuroimaging data. J Neurosci Methods 236, 19–25 (2014). [PubMed: 25117552]

39. Malik S et al. Histone deacetylase 7 and FoxA1 in estrogen-mediated repression of RPRM. Mol Cell Biol 30, 399–412 (2010). [PubMed: 19917725]

40. Allison MB et al. TRAP-seq defines markers for novel populations of hypothalamic and brainstem LepRb neurons. Molecular Metabolism 4, 299–309 (2015). [PubMed: 25830093]

41. Tannenbaum GS & Bowers CY Interactions of growth hormone secretagogues and growth hormone-releasing hormone/somatostatin. Endocrine 14, 21–27 (2001). [PubMed: 11322498]

42. Luo SX et al. Regulation of feeding by somatostatin neurons in the tuberal nucleus. Science 361, 76 (2018). [PubMed: 29976824]

43. Schick RR et al. Effect of galanin on food intake in rats: involvement of lateral and ventromedial hypothalamic sites. American Journal of Physiology-Regulatory, Integrative and Comparative Physiology 264, R355–R361 (1993).

44. Scharff AZ et al. Sex differences in IL-17 contribute to chronicity in male versus female urinary tract infection. JCI Insight 4, (2019).

45. Li L et al. Single-Cell RNA-Seq Analysis Maps Development of Human Germline Cells and Gonadal Niche Interactions. Cell Stem Cell 20, 858–873.e4 (2017). [PubMed: 28457750]

46. Petropoulos S et al. Single-Cell RNA-Seq Reveals Lineage and X Chromosome Dynamics in Human Preimplantation Embryos. Cell 165, 1012–1026 (2016). [PubMed: 27062923]

47. Herbison AE Somatostatin-immunoreactive neurones in the hypothalamic ventromedial nucleus possess oestrogen receptors in the male and female rat. Journal of neuroendocrinology 6, 323–8 (1994). [PubMed: 7920598]

48. Arnold AP & Chen X What does the 'four core genotypes' mouse model tell us about sex differences in the brain and other tissues? Front Neuroendocrinol 30, 1–9 (2009). [PubMed: 19028515]

49. Kow L-M & Pfaff DW Estrogen effects on neuronal responsiveness to electrical and neurotransmitter stimulation: an in vitro study on the ventromedial nucleus of the hypothalamus. Brain Research 347, 1–10 (1985). [PubMed: 2864983]

50. Minami T, Oomura Y, Nabekura J & Fukuda A 17β-Estradiol depolarization of hypothalamic neurons is mediated by cyclic AMP. Brain Research 519, 301–307 (1990). [PubMed: 1697776]

51. Zadran S et al. 17-β-Estradiol increases neuronal excitability through MAP kinase-induced calpain activation. Proc Natl Acad Sci USA 106, 21936 (2009). [PubMed: 19995977]

52. Armbruster BN, Li X, Pausch MH, Herlitze S & Roth BL Evolving the lock to fit the key to create a family of G protein-coupled receptors potently activated by an inert ligand. Proc Natl Acad Sci USA 104, 5163 (2007). [PubMed: 17360345]

53. Chen R, Wu X, Jiang L & Zhang Y Single-Cell RNA-Seq Reveals Hypothalamic Cell Diversity. Cell Rep 18, 3227–3241 (2017). [PubMed: 28355573]

54. Romanov RA et al. Molecular interrogation of hypothalamic organization reveals distinct dopamine neuronal subtypes. Nature Neuroscience 20, 176 (2016). [PubMed: 27991900]

55. Kim D-W et al. Multimodal Analysis of Cell Types in a Hypothalamic Node Controlling Social Behavior. Cell 179, 713–728.e17 (2019). [PubMed: 31626771]

56. Schulz DJ Plasticity and stability in neuronal output via changes in intrinsic excitability: it's what's inside that counts. J Exp Biol 209, 4821–7 (2006). [PubMed: 17142671]

57. McCarthy MM & Arnold AP Reframing sexual differentiation of the brain. Nature Neuroscience 14, 677–683 (2011). [PubMed: 21613996]

58. Forger NG, Strahan JA & Castillo-Ruiz A Cellular and molecular mechanisms of sexual differentiation in the mammalian nervous system. Front Neuroendocrinol 40, 67–86 (2016). [PubMed: 26790970]

59. Chartoff EH & Mavrikaki M Sex Differences in Kappa Opioid Receptor Function and Their Potential Impact on Addiction. Frontiers in Neuroscience 9, 466 (2015). [PubMed: 26733781]

60. Ferran JL, Puelles L & Rubenstein JLR Molecular codes defining rostrocaudal domains in the embryonic mouse hypothalamus. Frontiers in Neuroanatomy 9, 46 (2015). [PubMed: 25941476]

61. Consortium GTEx. The Genotype-Tissue Expression (GTEx) project. Nat Genet 45, 580–585 (2013). [PubMed: 23715323]

62. Burgoyne PS & Arnold AP A primer on the use of mouse models for identifying direct sex chromosome effects that cause sex differences in non-gonadal tissues. Biology of sex differences 7, 68–68 (2016). [PubMed: 27999654]

63. Satija R, Farrell JA, Gennert D, Schier AF & Regev A Spatial reconstruction of single-cell gene expression data. Nat Biotechnol 33, 495–502 (2015). [PubMed: 25867923]

64. Blondel VD, Guillaume J-L, Lambiotte R & Lefebvre E Fast unfolding of communities in large networks. *Journal of Statistical Mechanics*: Theory and Experiment 2008, P10008 (2008).

65. Crane JD, Mottillo EP, Farncombe TH, Morrison KM & Steinberg GR A standardized infrared imaging technique that specifically detects UCP1-mediated thermogenesis in vivo. Molecular Metabolism 3, 490–494 (2014). [PubMed: 24944909]

66. Robbins E et al. Quantitative non-radioactive in situ hybridization of preproenkephalin mRNA with digoxigenin-labeled cRNA probes. Anat Rec 231, 559–62 (1991). [PubMed: 1793181]

67. McQuin C et al. CellProfiler 3.0: Next-generation image processing for biology. PLOS Biology 16, e2005970 (2018). [PubMed: 29969450]

68. Lein E, Hawrylycz M, Ao N et al. Genome-wide atlas of gene expression in the adult mouse brain. Nature 445, 168–176 (2007). [PubMed: 17151600]
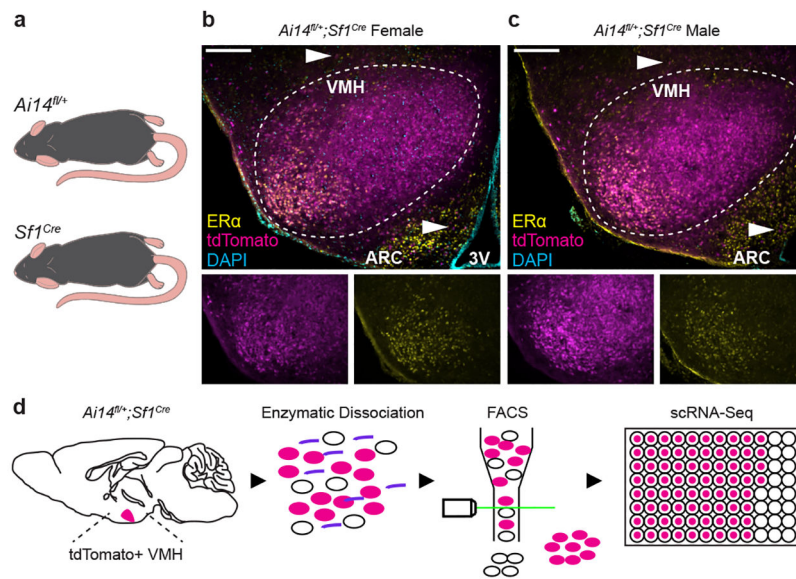
Figure 1. *Sf1* lineage tracing allows for targeted scRNA-seq of the VMH.
a, Strategy to fluorescently label neurons of the VMH using a Cre allele driven by the VMH lineage transcription factor, *Sf1*. **b,c,** Mice harboring both the *Sf1^{Cre}* allele and a latent allele of tdTomato (*Ai14*) show VMH specific fluorescence within the hypothalamus: coronal sections taken from P10 mice, scale bars = 200um. Both female mice (b, n = 3 animals) and male mice (c, n = 3 animals) show expression of ERα in the VMHvl. As expected, females show higher immunoreactivity. White arrowheads highlight scattered *Sf1* lineage cells outside of the VMH. **d,** Strategy for dissociation followed by FACS and VMH targeted scRNA-seq.
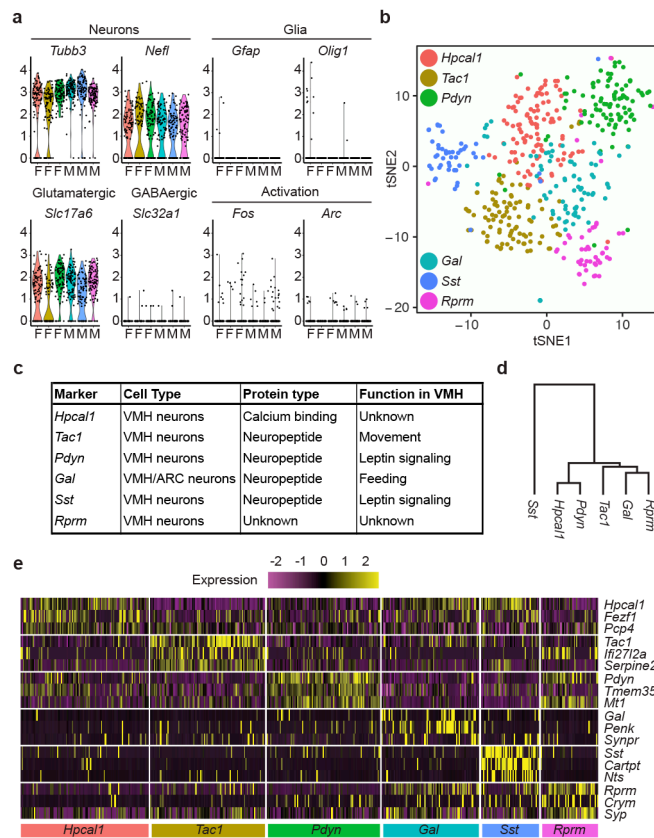
Figure 2. Single cell RNA sequencing reveals non-overlapping gene expression signatures in the VMH.

a, scRNA sequencing results from (n = 3 female mice (F), n = 3 male mice (M)) P10 mice showing high expression levels (given as $\log_e$((counts per 10k)+1)) of the neuron specific markers *Tubb3* and *Nefl*, with only scattered cells expressing the glial markers *Gfap* and *Olig1*. Cells also express high levels of the glutamatergic marker *Slc17a6*, low levels of the GABAergic marker *Slc32a1*, and limited expression of the immediate early genes *Fos* and *Arc*. **b,** tSNE showing clusters as defined by marker with highest expression relative to other clusters. **c,** Table showing predicted localization, protein type, and known function of cluster-defining markers. **d,** Hierarchical clustering tree showing relatedness of clusters based on transcriptional signatures. **e,** Heatmap showing expression of top three differentially expressed (with respect to all other clusters) markers for each cluster. Each vertical line represents a single cell, all 530 cells passing quality filtering are shown.
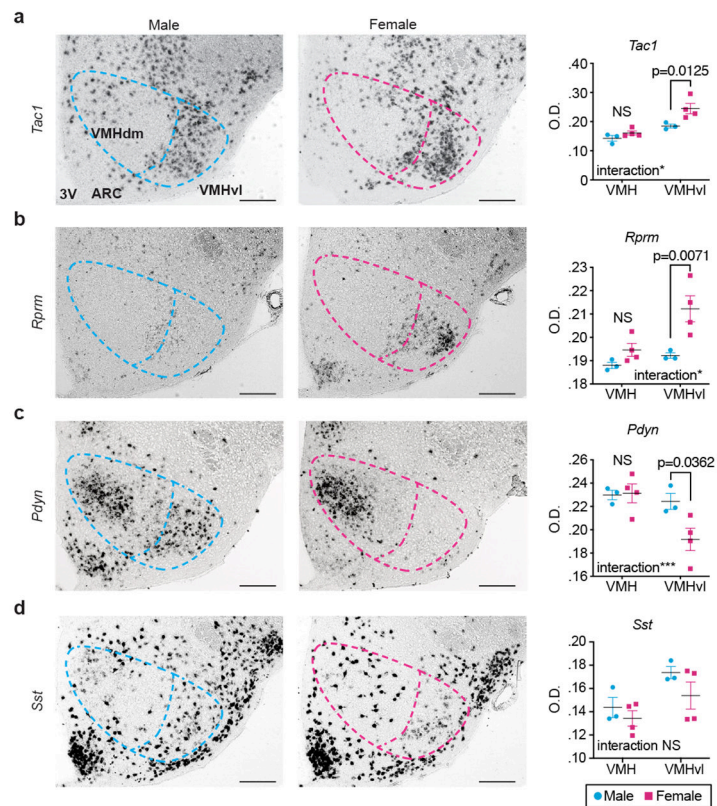
Figure 3. *Tac1*, *Rprm*, and *Pdyn* are sexually dimorphic genes in the adult VMHvl.
Spatial organization of cluster markers **a,** *Tac1*, **b,** *Rprm*, **c,** *Pdyn*, and **d,** *Sst* in the VMH of intact male (n = 3 animals) and female (n = 4 animals) mice by chromogenic ISH. mRNA levels were quantified within the VMH and VMHvl subregion (centre bars = mean, error bars = standard error). Two way ANOVA shows statistically significant interaction between sex and ROI for *Tac1* ($F(1,5) = 8.932, p = 0.0305$), *Rprm* ($F(1,5) = 13.23, p = 0.0149$), and *Pdyn* ($F(1,5) = 65.84, p = 0.0005$). Post-hoc Sidak's multiple comparison tests revealed statistically significant sex differences in expression in the VMHvl ($p = 0.0125$ for Tac1, $p = 0.0071$ for Rprm, $p = 0.0362$ for Pdyn) (Full ANOVAs in Supplementary Table 1). Dashed line shows boundary of VMH and VMHvl, in blue for male and magenta for female. Scalebars = 200μm.
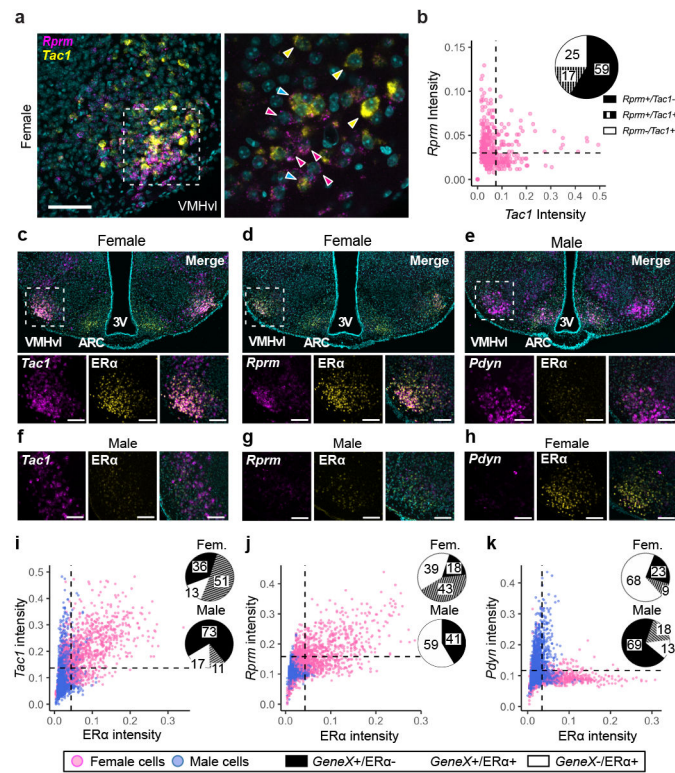
Figure 4. Sex biased transcripts are restricted to the ventrolateral VMH.
a, *Tac1* and *Rprm* transcripts in the female VMHvl (dashed box). Increased magnification of the VMHvl shows cells expressing *Rprm* alone (magenta arrowheads), *Tac1* alone (yellow arrowheads), or both (cyan arrowheads). **b,** Median pixel intensity for *Tac1* and *Rprm* transcripts in individual cells of the VMHvl (n = 560 cells from 3 female mice) showing 58.6% of cells express only *Rprm*, 24.8% express only *Tac1*, and 16.6% express both *Rprm* and *Tac1*. **c,** *Tac1* (magenta) together with ERα immunoreactivity (yellow) in the **c,** female or **f,** male VMHvl. **i,** Median pixel intensity for ERα and *Tac1* co-expression in cells from the VMHvl of females (n = 2944 cells from 5 mice) or males (n = 2330 cells from 6 mice). In females, 58.8% of *Tac1*+ cells also express ERα. Relatively limited expression of ERα is observed in the VMHvl of adult males. **d,** *Rprm* transcripts (magenta) together with ERα immunoreactivity (yellow) in the VMHvl of females or **g,** males. **j,** Median pixel intensity for ERα and *Rprm* in VMHvl cells from females (n = 2751 cells from 4 mice) and males (n = 1163 cells from 4 mice). In females, 70.3% of *Rprm*+ cells also express ERα. Limited expression of *Rprm* or ERα is observed in males. **e,** *Pdyn* (magenta) transcripts with ERα immunoreactivity (yellow) in the VMHvl of males or **h,** females. **k,** Quantification of ERα and *Pdyn* in VMHvl sections from females (n = 2051 cells from 5 mice) and males (n = 3105 cells from 6 mice). Limited (8.9% in females, 17.7% in males) co-expression of ERα and *Pdyn* is observed, as males express high levels of *Pdyn* and low levels of ERα whereas females express low levels of *Pdyn* and high levels of ERα. Dashed lines in **b, i-k** indicate positive/negative cutoffs (see Experimental Procedures). Percentages were determined from the total number of cells that express either ERα or the gene of interest or both (pie chart insets). Scalebars = 100μm.
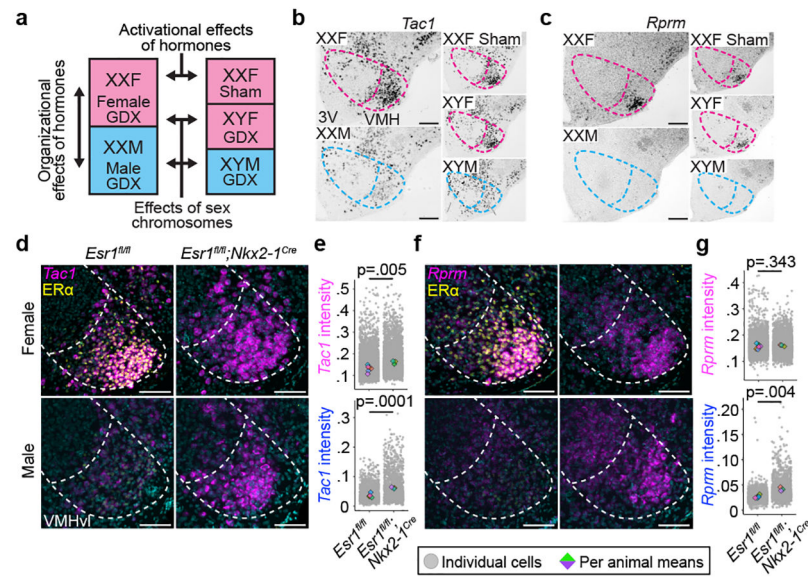
Figure 5. Female biased gene expression is established organizationally during development in the VMH.

a, Schematic of comparisons made with the "four-core genotypes" model to determine if sex differences arise from gonad or sex chromosome effects. **b,** *Tac1* transcripts in four core model (n = 2 animals for all GDX panels, n = 3 animals for sham panel) demonstrating that sex differences are permanently patterned (organizational effect) by gonadal hormones during development. **c,** *Rprm* transcripts in four core model (n = 2 animals for all GDX panels, n = 3 animals for sham panel) demonstrating that sex differences are also patterned by gonadal hormones during development. **d,** *Tac1* transcripts (magenta) together with ERα immunoreactivity (yellow) in the VMHvl of female and male *Esr1^{fl/fl}* (control) or *Esr1^{fl/fl}; Nkx2–1^{Cre}* (hypothalamic ERα knockout) animals. **e,** Median intensity of *Tac1* signal in individual VMHvl cells from female mice (n = 7904 cells from 6 CTL animals, 4402 cells from 3 KO animals) and male mice (n = 2409 cells from 5 CTL animals, 1576 cells from 3 KO animals). In females, developmental loss of ERα in the *Nkx2–1* lineage results in a significant (*t = 4.0384, df = 6.9088, p=.005*) increase in *Tac1* expression. In males, developmental loss of ERα in the *Nkx2–1* lineage results in a significant (*t = 8.0168, df = 5.6343, p=.0001*) increase in VMHvl *Tac1* expression. **f,** *Rprm* transcripts (magenta) together with ERα immunoreactivity (yellow) in the VMHvl of female and male *Esr1^{fl/fl}* or *Esr1^{fl/fl}; Nkx2–1^{Cre}* mice. **g,** Median intensity of *Rprm* signal in individual VMHvl cells from female (n = 6024 cells from 5 CTL animals, 3459 cells from 3 KO animals) and male (n = 2506 cells from 5 CTL animals, 1590 cells from 3 KO animals) mice. In females, developmental loss of ERα in the *Nkx2–1* lineage does not significantly alter VMHvl *Rprm* expression (t=1.0179, df=6.7578, p=0.34). In males, developmental loss of ERα in the *Nkx2–1* lineage results in a significant (t=6.3362, df=3.7439, p=.004) increase in VMHvl *Rprm* expression. Significance of gene expression differences determined by two-sided t-tests. All significance testing done on per-animal means of median fluorescence values (diamonds overlaying f,g). Scalebars = 100μm.
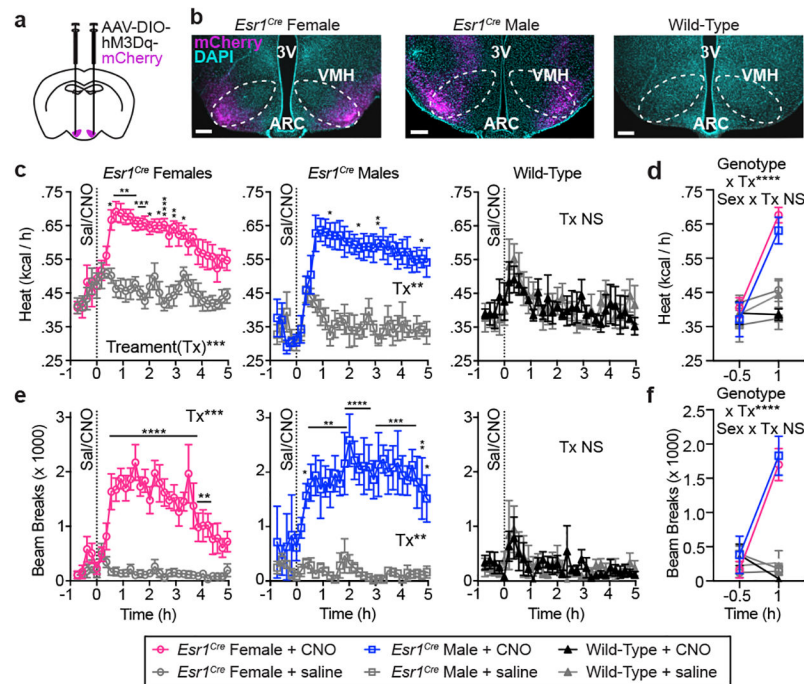
Figure 6. Specific activation of *Esr1*⁺ neurons in the VMHvl causes enhanced movement and thermogenesis in male and female mice.

a, AAV harboring the CRE dependent hM3Dq DREADD was stereotaxically delivered to the VMHvl of male and female mice. **b,** Female and male *Esr1*^*Cre*^ mice show mCherry fluorescence in the VMHvl indicating transduction and recombination of the AAV-DREADD; equivalently manipulated wild-type littermates do not. **c,** Female (n = 7 animals) *Esr1*^*Cre*^ mice show increased heat generation after CNO injection, compared to saline injection on a different day. Two-way RM ANOVA: *treatment: $F_{(1,2)}=27.06$, p=.0002; time: $F_{(7.040,84.48)}=7.905$, p<.0001; interaction: $F_{(32,384)}=5.779$, p<.0001*. Male (n = 4 animals) *Esr1*^*Cre*^ mice showed increased heat generation after CNO injection, compared to saline injection on a different day. Two-way RM ANOVA: *treatment: $F_{(1,6)}=19.76$, p=.0044; time: $F_{(4.749,28.49)}=10.96$, p<.0001; interaction: $F_{(32,192)}=9.422$, p<.0001)*. Wild-type mice (n = 5 animals: 3 female, 2 male) given AAV-FLEX-hM3Dq-mCherry showed no significant effect of time, treatment, or interaction of time and treatment. **d,** Cross group comparison of heat production 0.5 h before and 1 h after injection. After CNO injection, *Esr1*^*Cre*^ males and females exhibit similar significant increases in heat production. Three-way ANOVA: *genotype: $F_{(1,12)}=19.75$, p=.0008; sex: $F_{(1,12)}=6.599$, p=.025; treatment: $F_{(1,12)}=14.31$, p=.0026; interaction of genotype and treatment: $F_{(1,12)}=33.52$, p<.0001, but no significant interaction of either genotype or treatment with sex)*. **e,** Female (n = 7 animals) *Esr1*^*Cre*^ mice showed increased movement after CNO injection compared to saline injection on a different day. Two-way RM ANOVA: *treatment:$F_{(1,6)}=66.84$, p=.0002; time:$F_{(32,192)}=6.68$, p<.0001; interaction:$F_{(32,192)}=7.36$, p<.0001)*. Male (n = 4 animals) *Esr1*^*Cre*^ mice showed increased movement after CNO injection, compared to saline injection on a different day. Two-way RM ANOVA: *treatment: $F_{(1,3)}=41.32$, p=.0076; time: $F_{(32,96)}=1.881$, p<.0099; interaction: $F_{(32,96)}=2.45$, p=.0004)*. Wild-type mice (n = 5 animals: 3 female, 2 male) showed a significant effect of time (two-way RM ANOVA: *time:*

F(32,128)=1.732, p=.0171) but no effect of treatment, or interaction of time and treatment. **f,** Cross group comparison of movement 0.5 h before and 1 h after injection. After CNO injection, *Esr1^{Cre}* males and females exhibit similar significant increases in movement. Three-way ANOVA: *genotype: F(1,12)=23.63, p=.0004; treatment: F(1,12)=23.36, p=.0004; interaction between genotype and treatment: F(1,12)=37.95, p<.0001, but no significant effect of sex, or interaction of either genotype or treatment and sex.* All subjects were 10–18 weeks old and singly housed in indirect calorimetry chambers. For all graphs, centre value = mean, error bars = standard error. Post-hoc Sidak's multiple comparison tests were used for pairwise comparisons: * = p<0.05, ** = p<0.01, *** = p<0.001, **** = p<0.0001 (Full ANOVAs in Supplementary Table 1). Scale bars = 100μm. Vertical dashed line at x = 0 denotes time of injection with CNO or saline.
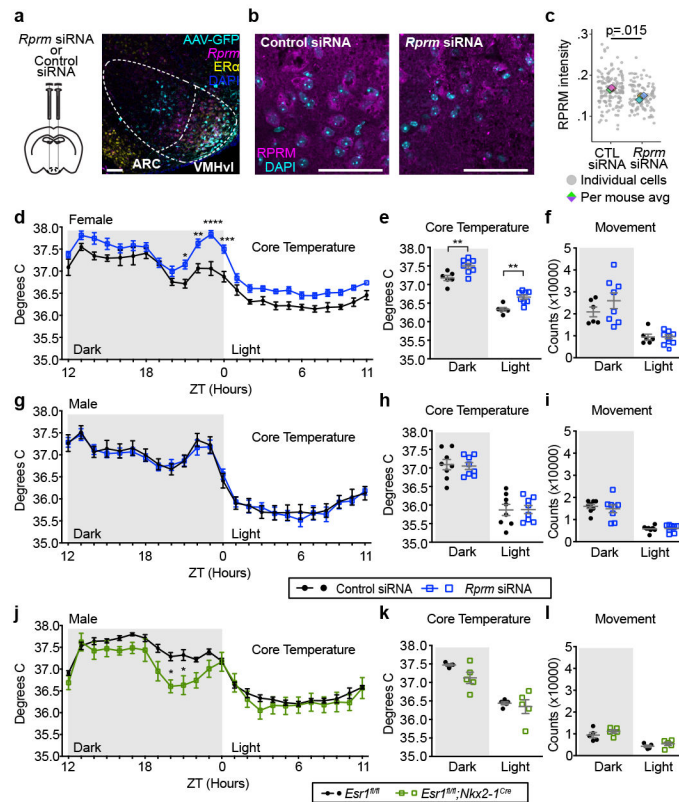
Figure 7. Temperature is dysregulated in female but not male mice lacking *Rprm*.
a, Stereotaxic injection was used to deliver cell-permeable siRNA pools either targeting *Rprm* or non-targeting to the VMHvl of female mice. AAV-GFP was used to validate specific targeting of the VMHvl by the stereotaxic coordinates used **b,** IHC shows partial depletion of RPRM protein in the VMHvl. **c,** Quantification of IHC images confirms significant depletion of RPRM in female mice injected with *Rprm* targeting siRNA pools (n = 3 animals) compared to female mice injected with non-targeting siRNAs (n = 3 animals; two-sided t-test, t = 5.579, df = 2.6639, p = 0.015). **d,** Core temperature is higher in female mice injected with *Rprm* targeting siRNA pools (n = 8 animals) compared to female mice injected with non-targeting siRNA pools (n = 6 animals). Two way RM ANOVA: Interaction (*F(23,276) = 1.653, p = 0.0329)*, Time *(F(23,276) = 67.31, p <0.0001)*, siRNA *(F(1, 12) = 18.31, p = 0011)*. **e,** the effect of *Rprm* depletion on core temperature is significant in both the inactive (day) phase and active (night) phase compared to non-targeting controls. Two way RM ANOVA: Interaction (*F(1,12) = 1.653, p = 0.9408)*, Time *(F(1,12) = 330.1, p <0.0001)*, siRNA *(F(1, 12) = 18.31, p = .0011)*. **f,** *Rprm* depletion did not affect movement in females in the inactive or active phases when compared to non-targeting controls. The same animals were used for all measurements in d-f. **g,** in males, core temperature is not significantly altered in mice injected with *Rprm* targeting siRNA pools (n = 8 animals) compared to mice injected with non-targeting siRNA pools (n = 8 animals). Two way RM ANOVA: Interaction (*F(1, 14) = 0.3953, p = 0.5396)*, Time *(F(1,14) = 953.2, p <0.0001)*, siRNA *(F(1, 14) = .0069, p = 0.9349)*. **h,i,** The effect of *Rprm* depletion on core temperature is not significant in the inactive or active phases compared to non-targeting controls. The same animals were used for all measurements in g-i. **j,** Male mice that express *Rprm* in the

VMHvl due to developmental ablation of hypothalamic ERα (*Esr1^{fl/fl}; Nkx2–1^{Cre}*, n = 5 animals), show decreased core body temperature compared to littermate (*Esr1^{fl/fl}*, n = 5 animals) controls during some times of the active phase. When averaged over the entire night or day, there is a significant effect of the interaction between genotype and time of day, but not genotype alone on **k,** core body temperature (Two way RM ANOVA: Interaction $(F_{(1,8)} = 5.848$, p = 0.0420), Time of day $(F_{(1,8)} = 287.8$, p = *<0.0001, Genotype $(F_{(1,8)} =$ 1.771, p = 0.2200).* **l,** No effect on movement was observed in *Esr1^{fl/fl}; Nkx2–1^{Cre}* mice compared to littermate controls (Two way RM ANOVA: Interaction $(F_{(1,8)} = 0.3247$, p = 0.5845), Time of day $(F_{(1,8)} = 118.2$, p = *<0.0001, Genotype $(F_{(1,8)} = 1.531$, p = 0.2511).* The same animals were used for all measurements in j-l. Post-hoc Sidak's multiple comparison tests were used for pairwise comparisons: * = p<0.05, ** = p<0.01, *** = p<0.001, **** = p<0.0001 (Full ANOVAs in Supplementary Table 1). For all graphs, centre value = mean, error bars = standard error. Scalebars = 100μm.